Vitamin C Promotes Epidermal Proliferation by Promoting DNA Demethylation of Proliferation-Related Genes in Human Epidermal Equivalents

Yasunori Sato[1], Ayami Sato[2], Florence[3], Akari Kuwano[3], Yasunari Sato[3], Hideki Tanaka[1,4], Toshiyuki Kimura[1], Tsuyoshi Ishii[3] and Akihito Ishigami[2]

Journal of Investigative Dermatology (2025) **145,** 2775–2788; doi:10.1016/j.jid.2025.03.040

Keratinocyte differentiation is highly regulated to produce the stratified structure of the epidermis and must be balanced with cell proliferation. Our prior studies revealed that hairless mice that cannot synthesize vitamin C (VC) exhibit epidermal atrophy. VC is a cofactor for the DNA demethylation (ten-eleven translocation) enzyme, but the role of VC in DNA demethylation during keratinocyte differentiation remains unclear. In this study, we evaluated the role of VC in epigenetic regulation of epidermal proliferation and differentiation in a human epidermal equivalent model. Our findings demonstrated that intracellular VC uptake increased epidermal thickness, cell proliferation, and global levels of 5-hydroxymethylcytosine DNA. Notably, these effects of VC were attenuated by an inhibitor of the ten-eleven translocation enzyme. DNA microarray and whole-genome bisulfite sequencing analyses revealed that 12 genes related to cell proliferation were significantly upregulated by VC. Furthermore, hypomethylated DNA regions associated with these genes were revealed in the presence of VC. Collectively, our findings provide insight into how VC increases epidermal thickness by promoting keratinocyte proliferation through the DNA demethylation of proliferation-related genes. VC is a promising molecule that can be used as developing treatment for epidermal thinning, including in aging.

Keywords: Aging, Keratinocytes, Skin health, Skin structure and function

INTRODUCTION

The epidermis is a unique, highly regulated layered tissue consisting of cells at different stages of differentiation (Henry et al, 2012). Keratinocytes make up most of the epidermis and proliferate in the basal cell layer (Morizane et al, 2023). After differentiating in the basal layer, keratinocytes migrate upward through the stratum spinosum, stratum granulosum, and stratum corneum (SC) (Eckhart et al, 2013). Eventually, differentiated cells are shed from the epidermal surface (Eckhart et al, 2013). Keratinocytes express a strictly regulated number of differentiation genes (Mulder et al, 2012), including keratin (K) 14 gene *K14* in the basal layer, *K1/K10* in the spinous layer, and loricrin gene *LOR* and filaggrin gene *FLG* in the granular layer (Henry et al, 2012; Ramos-e-Silva and Jacques, 2012). Expression abnormalities in these genes result in disrupted skin structure and function.

The epidermal barrier prevents water loss and protects against damage such as from UVR, chemicals, and microorganisms (Ramos-e-Silva and Jacques, 2012). Aging leads to the breakdown of these essential functions, increasing the susceptibility of the skin to damage (Choi, 2019). The skin epidermis also serves as a typical visual indicator of the aging process.

L-ascorbic acid (vitamin C [VC]) is widely recognized for its antioxidant properties in the skin (Masaki, 2010). We previously demonstrated that VC enhances collagen synthesis (Kishimoto et al, 2013), alleviates UV-induced damage to the epidermis (Kawashima et al, 2018), and inhibits melanin deposition (Sato et al, 2017). We found that long-term VC deficiency leads to epidermal atrophy in a mouse model with disrupted VC synthesis capabilities (Sato et al, 2012). Other groups have also reported that VC promoted keratinocyte viability, induced expression of differentiation marker genes, and increased SC barrier lipids in monolayer or organotypic cultures of normal human keratinocytes (Boyce et al, 2002; Michalak et al, 2021). Together, these data suggest that VC regulates epidermal cell proliferation and differentiation.

[1]*Faculty of Pharmaceutical Sciences, Hokuriku University, Kanazawa, Japan;* [2]*Molecular Regulation of Aging, Tokyo Metropolitan Institute for Geriatrics and Gerontology, Tokyo, Japan; and* [3]*ROHTO Pharmaceutical, Osaka, Japan*

[4]*Present address: Department of Pharmacy, University of Fukui Hospital, Fukui, Japan*

Correspondence: Akihito Ishigami, Molecular Regulation of Aging, Tokyo Metropolitan Institute for Geriatrics and Gerontology (TMIG), 35-2 Sakae-cho, Itabashi-ku, Tokyo 173-0015, Japan. E-mail: ishigami@tmig.or.jp

Abbreviations: 5-hmC, 5-hydroxymethylcytosine; 5-mC, 5-methylcytosine; DMR, differentially methylated region; ECL, epidermal cell layer; K, keratin; SC, stratum corneum; TET, ten-eleven translocation; VC, vitamin C; WGBS, whole-genome bisulfite sequencing

Received 23 October 2024; revised 25 March 2025; accepted 27 March 2025; accepted manuscript published online 20 April 2025; corrected proof published online 10 May 2025

One hypothesis is that VC regulates epidermal cell proliferation and differentiation through its role in DNA methylation (Blaschke et al, 2013; Minor et al, 2013). DNA methylation plays a critical role in regulating gene expression because it controls the accessibility of transcription machinery to DNA. DNA methyltransferases add a methyl group to the cytosine nucleotide in DNA. In contrast, ten-eleven translocation (TET) family enzymes convert 5-methylcytosine (5-mC) to 5-hydroxymethylcytosine (5-hmC) in the presence of VC (DiTroia et al, 2019; Young et al, 2015). VC was reported to increase 5-hmC levels in several cultured cell lines (Lin et al, 2014; Sajadian et al, 2016; Shenoy et al, 2017), and VC deficiency may decrease 5-hmC in some organs in vivo (Thaler et al, 2022). VC's epigenetic functions have been applied to improve the quality of reprogramming induced pluripotent stem cell and embryonic stem cell formation (DiTroia et al, 2019; Lee Chong et al, 2019). However, whether VC regulates epidermal cell proliferation and differentiation through DNA methylation changes has not been investigated.

This study investigated whether VC promotes epidermal cell proliferation and differentiation through epigenetic changes in a 3-dimensional cultured human epidermal equivalent model, which recapitulates the structure of the human epidermis. DNA microarray and whole-genome bisulfite sequencing (WGBS) analyses were conducted to identify genes whose expression is affected by VC through changes in DNA methylation. In this study, we show that VC increases the expression of proliferation-related genes through DNA demethylation and propose that VC may be able to be developed for combating the effects of aging and maintaining skin health.

RESULTS

VC promotes cell proliferation in a human epidermal equivalent model

To determine whether VC affects epidermal cell proliferation and differentiation through epigenetic changes in a human epidermal equivalent model, we first constructed a human epidermal equivalent model (Figure 1a). To avoid the influence of pH changes on the human epidermal equivalent model, we added VC sodium salt to the culture medium and changed the medium daily (Supplementary Figure S1a–d). Human blood VC levels can reach 0.1 mM or higher with oral supplementation (Padayatty et al, 2004). In healthy skin, VC is actively transported from blood vessels in the dermal layer to keratinocytes in the basal layer of the epidermis through sodium-dependent VC transporters (Pullar et al, 2017). VC concentrations in epidermal tissues are higher than in plasma, reaching 1.0 mM or more. Accordingly, VC concentrations of 1.0 and 0.1 mM were chosen to physiologically model average VC concentrations in human plasma and VC concentrations imported into the epidermis (Richelle et al, 2006). A VC concentration of 1.0 mM in culture medium was previously shown to alter several cellular functions in vivo (Cimmino et al, 2017). Human epidermal equivalent models were successfully constructed, and supplementation with VC for 7 and 14 days allowed evaluation of short- and longer-term impacts of VC (Figure 1b). The SC was observed in the 0.1- and 1.0-mM VC–treated human epidermal equivalents after 7 days with no discernible difference in thickness compared with that in untreated human epidermal equivalents (Figure 1b and c). However, the epidermal cell layer (ECL) exhibited significantly increased thickness in the 0.1- and 1.0-mM VC–treated epidermal models at this time point. After 14 days, SC thickness was significantly lower in human epidermal equivalents treated with 1.0 mM VC than in those without VC (Figure 1b and c). The ECL increased in thickness with increasing VC concentrations. These findings suggest that VC promotes epidermal tissue formation in human epidermal equivalents.

VC is widely recognized to exert antioxidant properties and function in the skin when present as a cofactor in its reduced form (L-ascorbic acid) (Pullar et al, 2017). Therefore, we measured the levels of L-ascorbic acid and its oxidized form (dehydroascorbic acid) in human epidermal equivalents. VC was present in human epidermal equivalents, with the majority being in the L-ascorbic acid form (Figure 1d). We measured cell viability in the human epidermal equivalents and found significantly greater viability in the 1.0-mM VC–treated epidermis than in the untreated epidermis after culturing for 7 and 14 days (Figure 1e). Because these phenotypic changes occurred in the presence of VC sodium salt, we next confirmed that the changes were due to the VC by constructing human epidermal equivalents in the presence of 0.1- and 1.0-mM sodium. Indeed, the observed phenotypic changes did not occur in just the presence of sodium but also did occur in the presence of VC (Supplementary Figure S2a–c).

To investigate whether VC increases keratinocyte differentiation during epidermal tissue formation, we examined differentiation markers specific to each epidermal layer. These included collagen IV in basement membrane, K14 in basal layer, K1/K10 in spinous layer, and filaggrin and loricrin in granular layer. All differentiation markers were detected in the appropriate layers of the human epidermal equivalents after 7 and 14 days of culture with or without VC (Figure 1f). We used immunofluorescence staining to also investigate the number of Ki-67–positive proliferative cells, which were detected in the basal layers of the human epidermal equivalents (Figure 1g). A higher number of Ki-67–positive cells was present at 7 than at 14 days of culture, and there were significantly more Ki-67–positive cells with increasing concentrations of VC at both 7 and 14 days (Figure 1h). Together, these findings suggest that VC promotes the proliferation of keratinocytes, potentially leading to the thickening ECL observed in the presence of VC.

VC treatment increases global DNA demethylation in a human epidermal equivalent model

We next explored the mechanism underlying the observed increase in proliferation in VC-treated human skin equivalents. Because VC has been identified as a cofactor for DNA demethylation enzymes, we investigated the effect of VC on global DNA methylation by detecting 5-mC and 5-hmC levels after 7 and 14 days of culture using dot blot analysis. The levels of 5-mC in the 0.1- and 1.0-mM VC–treated human epidermal equivalents did not significantly change at 7 or 14 days compared with those in the untreated human epidermal equivalents (Figure 2a and b). However, 5-hmC

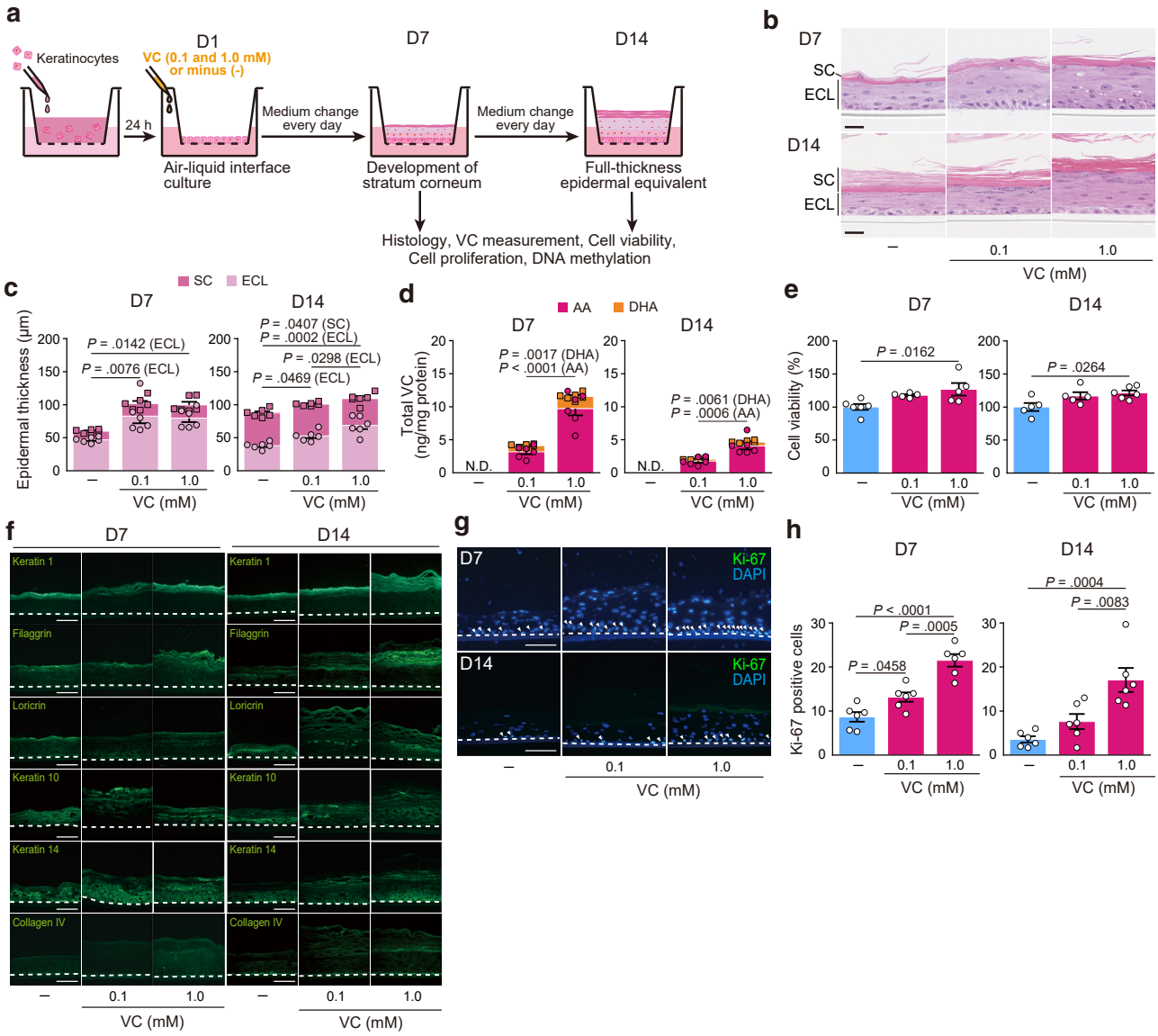

Figure 1. VC promotes cell proliferation in human epidermal equivalents. (**a**) Experimental outline for testing the effect of VC on epidermal cell proliferation and differentiation. (**b**) Representative H&E images of the human epidermal equivalents after 7 and 14 days of culture in the presence or absence of VC. Bars = 50 μm. (**c**) Quantification of SC (dark pink) and ECL (light pink) thickness in human epidermal equivalents (n = 6). (**d**) Total VC concentrations in the human epidermal equivalents, including AA (red) and DHA (orange) (n = 6). (**e**) Cell viability of human epidermal equivalents treated with (red) or without (blue) VC for 7 and 14 days (n = 5–6). (**f**) Representative immunofluorescence images showing keratin 1, filaggrin, loricrin, keratin 10, keratin 14, and collagen IV. Bars = 50 μm. (**g**) Representative immunofluorescence images showing Ki-67, a marker of proliferative cells, and DAPI. Arrowheads indicate Ki-67–positive cells. Bars = 20 μm. (**h**) Quantification of Ki-67–positive cells in the human epidermal equivalents (n = 6). The dotted line represents the basement membrane. Data for all bar graphs are presented as the mean ± SEM. Significance was determined by 1-way ANOVA with Tukey's posthoc test (for **c**–**e** and **h**). Source data are provided as a Source Data file. AA, ascorbic acid; DHA, dehydroascorbic acid; ECL, epidermal cell layer; h, hour; N.D., not detected; SC, stratum corneum; VC, vitamin C.

levels drastically increased in 0.1- and 1.0-mM VC–treated human epidermal equivalents after 7 (5.3- and 6.2-fold greater, respectively, compared with untreated one) and 14 (7.1- and 7.1-fold greater, respectively, compared with untreated ones) days of culture (Figure 2c and d). We used immunofluorescence to confirm the dot blot results, finding no discernible differences in the number of 5-mC–positive cells between the VC-treated and -untreated epidermis (Figure 2e and f). In contrast, the number of 5-hmC–positive cells significantly increased with increasing concentrations of VC at 7 and 14 days (Figure 2g and h). We also confirmed that addition of 0.1- or 1.0-mM sodium did not significantly change the 5-mC or 5-hmC levels in the human epidermal equivalents (Supplementary Figure S3a–d). These results indicate that VC facilitates DNA demethylation in human epidermal equivalents.

VC-induced DNA demethylation correlates with increased ECL thickness and cell proliferation in human epidermal equivalents

After determining that VC induces DNA demethylation, we investigated whether this effect impacts ECL thickening and epidermal cell proliferation. We constructed human epidermal equivalents with and without 1.0 mM VC in the

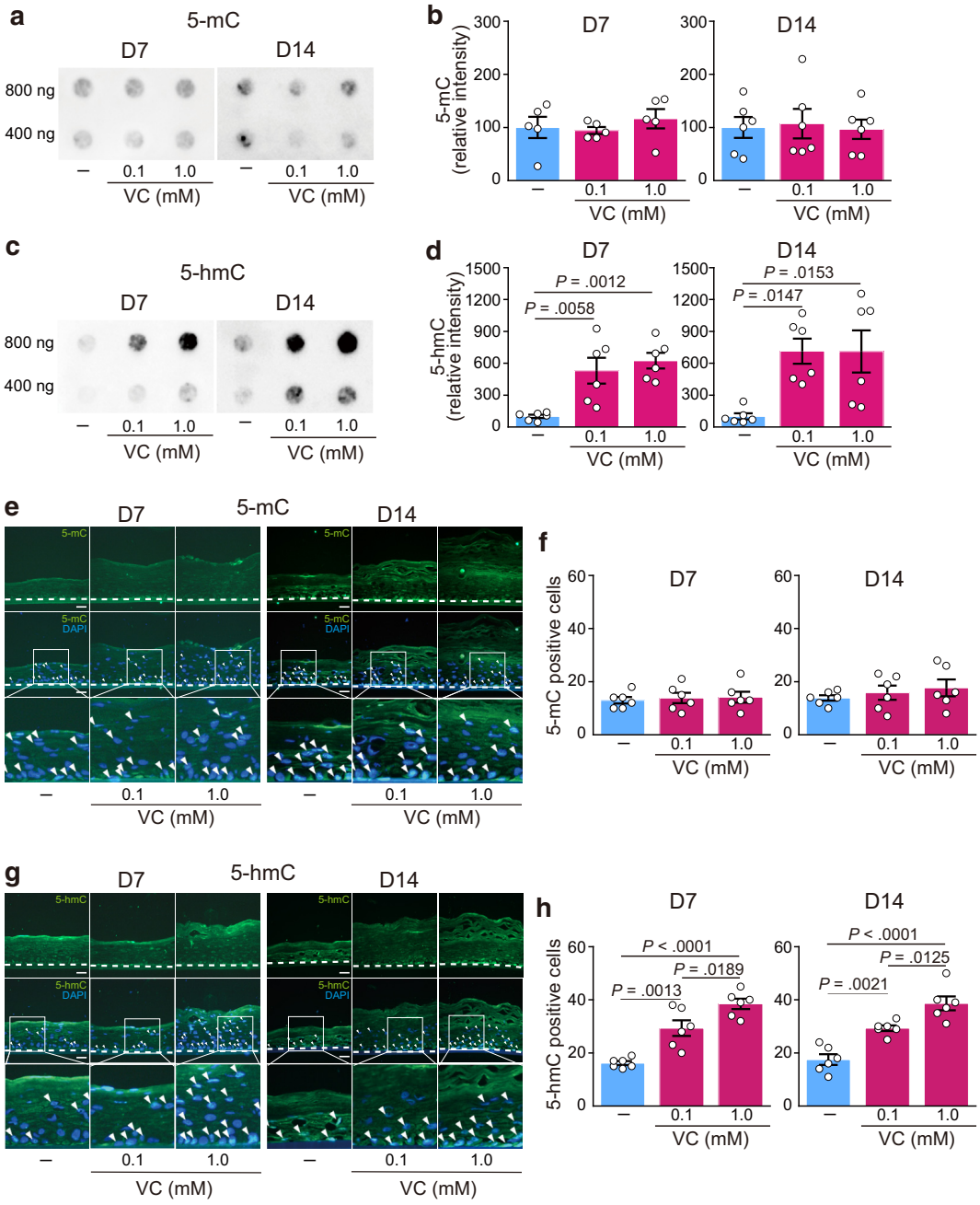

Figure 2. VC increases 5-hmC levels in human epidermal equivalents. (**a**) Representative dot blot images of 5-mC at 7 and 14 days after treatment with or without VC. (**b**) Semiquantitative analysis of 5-mC dot blots of 800 ng of genomic DNA (n = 5–6). Quantification was performed with Multi Gauge V3.0 software. (**c**) Representative dot blot images of 5-hmC at 7 and 14 days after treatment with or without VC. (**d**) Semiquantitative analysis of 5-hmC dot blots of 800 ng of genomic DNA (n = 6). (**e**) Representative immunofluorescence images showing 5-mC. (**f**) Quantification of 5-mC–positive cells in the human epidermal equivalents (n = 6). (**g**) Representative immunofluorescence images showing 5-hmC. (**h**) Quantification of 5-hmC–positive cells in the human epidermal equivalents (n = 6). Arrowheads indicate (**e**) 5-mC–positive cells and (**g**) 5-hmC–positive cells. Bars = 20 μm. The dotted line represents the basement membrane. For all the bar graphs, the data are presented as the mean ± SEM. The red and blue bars in the graphs represent treatment with and without VC, respectively (for **b**, **d, f,** and **h**). Significance was determined by 1-way ANOVA with Tukey's posthoc test (for **b**, **d, f,** and **h**). Source data are provided as a Source Data file. 5-hmC, 5-hydroxymethylcytosine; 5-mC, 5-methylcytosine; VC, vitamin C.

presence or absence of a TET inhibitor (Bobcat339) (Figure 3a). The choice of 1.0 mM VC was based on previous results; this concentration demonstrated more significant effects on DNA demethylation, cell viability, and cell proliferation. Compared with treatment with VC alone, cotreatment with VC and the TET inhibitor at 3.75 or 7.50 μM significantly decreased 5-hmC levels (Figure 3b and c) but not 5-mC levels (Figure 3d and e). Cotreatment with VC and the TET inhibitor reduced the thickness of the ECL and decreased cell viability (Figure 3f–h), resulting in phenotypic changes similar to those of the untreated epidermal equivalents. We also confirmed that the TET inhibitor alone did not significantly change cell viability (Figure 3h). These results indicate that TET inhibitor alone does not induce toxicity and that VC-

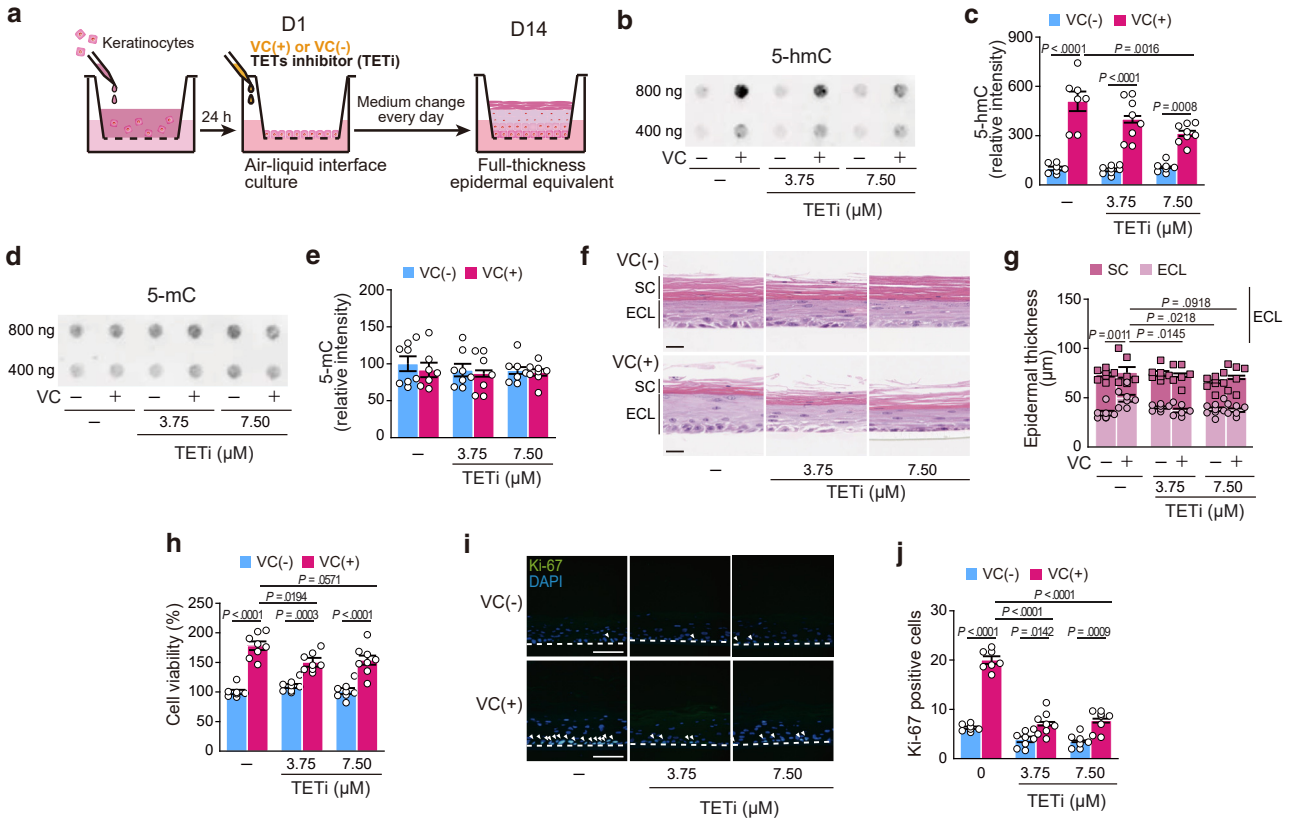

Figure 3. VC-induced DNA demethylation correlates with increased ECL thickness and cell proliferation in human epidermal equivalents. (**a**) Outline for experiments to test the effects of VC and a TET inhibitor on epidermal cell proliferation. (**b**) Representative dot blot images of 5-hmC in epidermal equivalents after 14 days of VC and TET inhibitor treatment. (**c**) Semiquantitative analysis of 5-hmC dot blots of 800 ng of genomic DNA (n = 7–8). Quantification was performed with Multi Gauge V3.0 software. (**d**) Representative dot blot images of 5-mC after 14 days of VC and TET inhibitor treatment. (**e**) Semiquantitative analysis of 5-mC dot blots of 800 ng of genomic DNA (n = 7–8). **f**) Representative H&E images of the human epidermal equivalents after 14 days of culture. Bars = 50 μm. (**g**) Quantification of SC (dark pink) and ECL (light pink) in the epidermal equivalents (n = 6–8). (**h**) Cell viability of epidermal equivalents after 14 days of VC and TET inhibitor treatment (n = 7–8). (**i**) Representative immunofluorescence images showing Ki-67, a marker of proliferating cells. Bars = 20 μm. (**j**) Quantification of Ki-67–positive cells in the human epidermal equivalents (n = 7–8). The dotted line represents the basement membrane. For all the bar graphs, the data are presented as the mean ± SEM. The red and blue bars in the graphs represent data collected with and without VC, respectively (for **c, e, h,** and **j**). Significance was determined by 1-way ANOVA with Tukey's posthoc test (for **c, e, g, h,** and **j**). TETi denotes TET inhibitor. Source data are provided as a Source Data file. 5-hmC, 5-hydroxymethylcytosine; 5-mC, 5-methylcytosine; ECL, epidermal cell layer; h, hour; SC, stratum corneum; TET, ten-eleven translocation; VC, vitamin C.

induced DNA demethylation promotes epidermal tissue formation in VC-treated human epidermal equivalents.

To determine whether VC-associated DNA demethylation affects differentiation or proliferation, we examined the expression of keratinocyte differentiation markers in human epidermal equivalents constructed with TET inhibitor. Keratinocyte differentiation markers were detected in the appropriate layers even in the presence of the TET inhibitor (Supplementary Figure S4). Cotreatment with VC and the TET inhibitor significantly reduced the number of proliferative cells in the basal layer (Figure 3i and j). The results indicate that VC-induced DNA demethylation associates with the ECL thickening and increased proliferation seen in VC-treated human epidermal equivalents.

VC changes the transcriptional profile and enhances the expression of cell proliferation–related genes in human epidermal equivalents

We next conducted a microarray analysis to determine the transcriptional profiles of human epidermal equivalents cultured with and without 1.0 mM VC for 14 days (Figure 4a). According to the results of principal component analysis, the presence of 1.0 mM VC in the human epidermal equivalents induced a change in the overall transcriptional profiles compared with the transcriptional profiles of those without VC (Figure 4b). Hierarchical cluster analysis allowed us to visualize the changed gene expression patterns in each human epidermal equivalent (Figure 4c). A total of 393 differentially expressed genes were identified in the human epidermal equivalents after 14 days of culture with VC, with a predominance of upregulated genes (283 upregulated genes vs 110 downregulated genes) (Figure 4d and e). We then performed gene set enrichment analysis using a total of 135,750 probes contained in the microarray, which included not only mRNA expression but also long noncoding RNAs and microRNAs. The top 10 sets of upregulated genes in the VC-treated and -untreated groups are shown in Figure 4f and g, respectively. VC increases the expression of genes involved in cell proliferation and DNA replication (Figure 4f and h). In contrast, the untreated epidermis showed upregulated

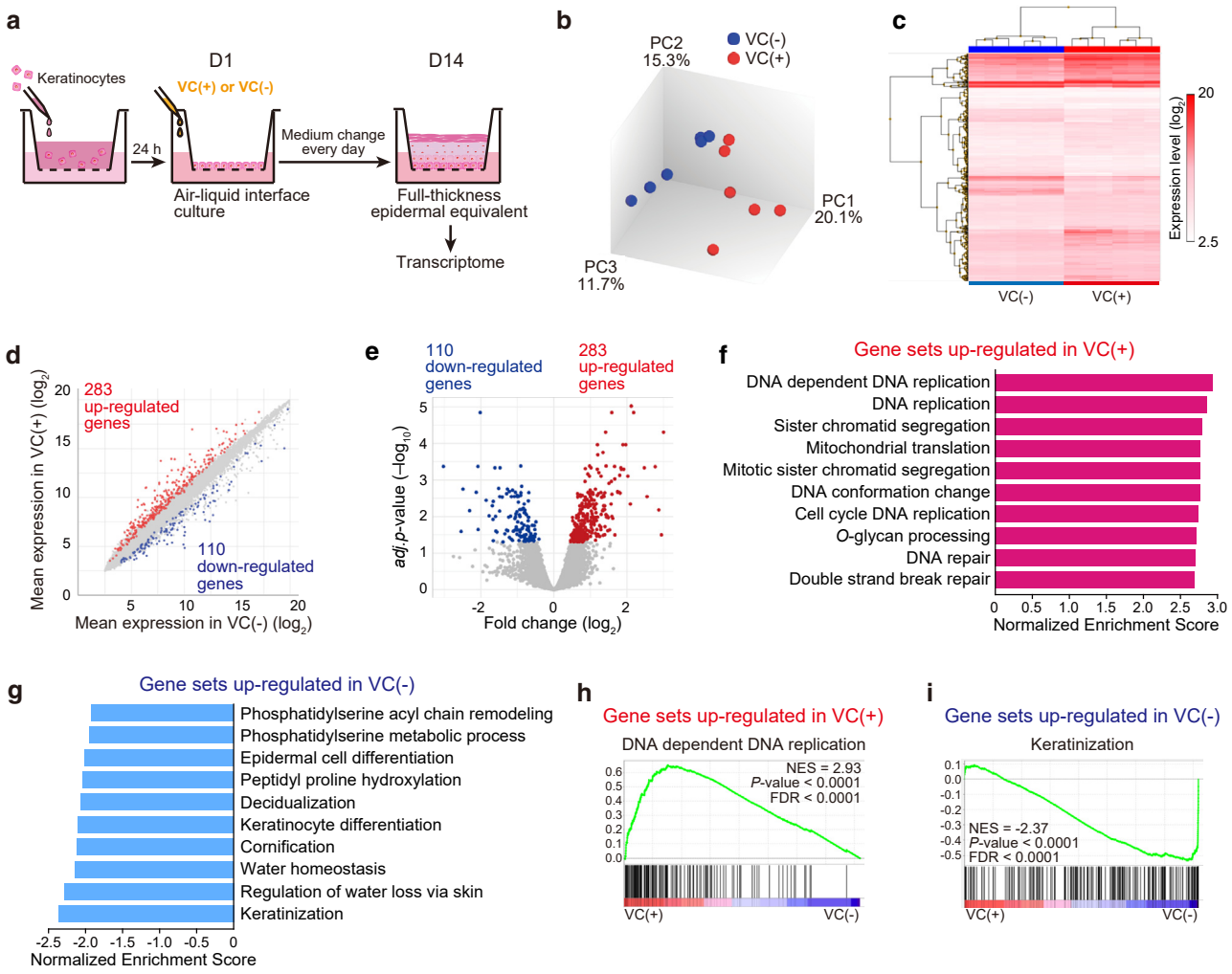

Figure 4. VC changes the transcriptional profile and enhances the expression of cell proliferation–related genes in human epidermal equivalents. (**a**) Experimental outline for testing the effect of VC on transcription. (**b**) Principal component analysis of the transcriptional profiles of VC(+) (red) and VC(−) (blue) human epidermal equivalents (n = 6). (**c**) Hierarchical cluster analysis of the transcriptional profiles of the human epidermal equivalents between the VC(+) and VC(−) groups. (**d**) Scatter plot of the transcriptional profiles of the VC(+) and VC(−) human epidermal equivalents. There were 283 changes in gene upregulation (red) and 110 changes in downregulation (blue) in the VC(+) group compared with those in VC(−). (**e**) Volcano plot of the transcriptional profiles of the VC(+) and VC(−) human epidermal equivalents. The 283 red and 110 blue dots represent genes whose expressions were significantly upregulated and downregulated, respectively, in the VC(+) group. (**f**) The top 10 gene sets of upregulated genes in the VC(+) group were related to cell proliferation. (**g**) The top 10 gene sets of upregulated genes in the VC(−) group were related to terminal differentiation. (**h**) Representative results after GSEA of the upregulated gene sets in VC(+) group. (**i**) Representative results after GSEA of the upregulated gene sets in the VC(−) group. GSEA, gene set enrichment analysis; h, hour; PC, principal component; VC, vitamin C.

expression of genes involved in terminal differentiation and skin barrier regulation (Figure 4g and i). These results indicate that the absence of VC leads to early differentiation, whereas the presence of VC promotes keratinocyte proliferation, resulting in delayed differentiation.

The microarray analysis indicated that gene expression levels of keratinocyte differentiation markers, such as *FLG*, *K1*, *K10*, loricrin gene *LOR*, and *K14*, were not significantly changed by VC treatment in human epidermal equivalents (Supplementary Figure S5a), consistent with our earlier immunofluorescence findings (Figure 1f). We further analyzed the microarray data to determine the expression levels of genes encoding TET enzymes and DNA methyltransferases. VC treatment did not affect the expression of TET enzyme genes (Supplementary Figure S5b), but *DNMT3A* and *DNMT3B* genes were significantly increased by VC treatment in human epidermal equivalents (Supplementary Figure S5c). Collectively, these findings indicate that VC promotes the expression of cell proliferation–related genes without affecting the differentiation-related genes and TET enzymes genes.

VC facilitates whole-genome DNA demethylation

To further elucidate the effect of VC on DNA methylation profiles, we conducted WGBS of human epidermal equivalents cultured with and without 1.0 mM VC for 14 days (Figure 5a). The overall DNA methylation profiles were distinct in human epidermal equivalents cultured with and without VC (Figure 5b and Supplementary Figure S6a). A total of 10,279 differentially methylated regions (DMRs)

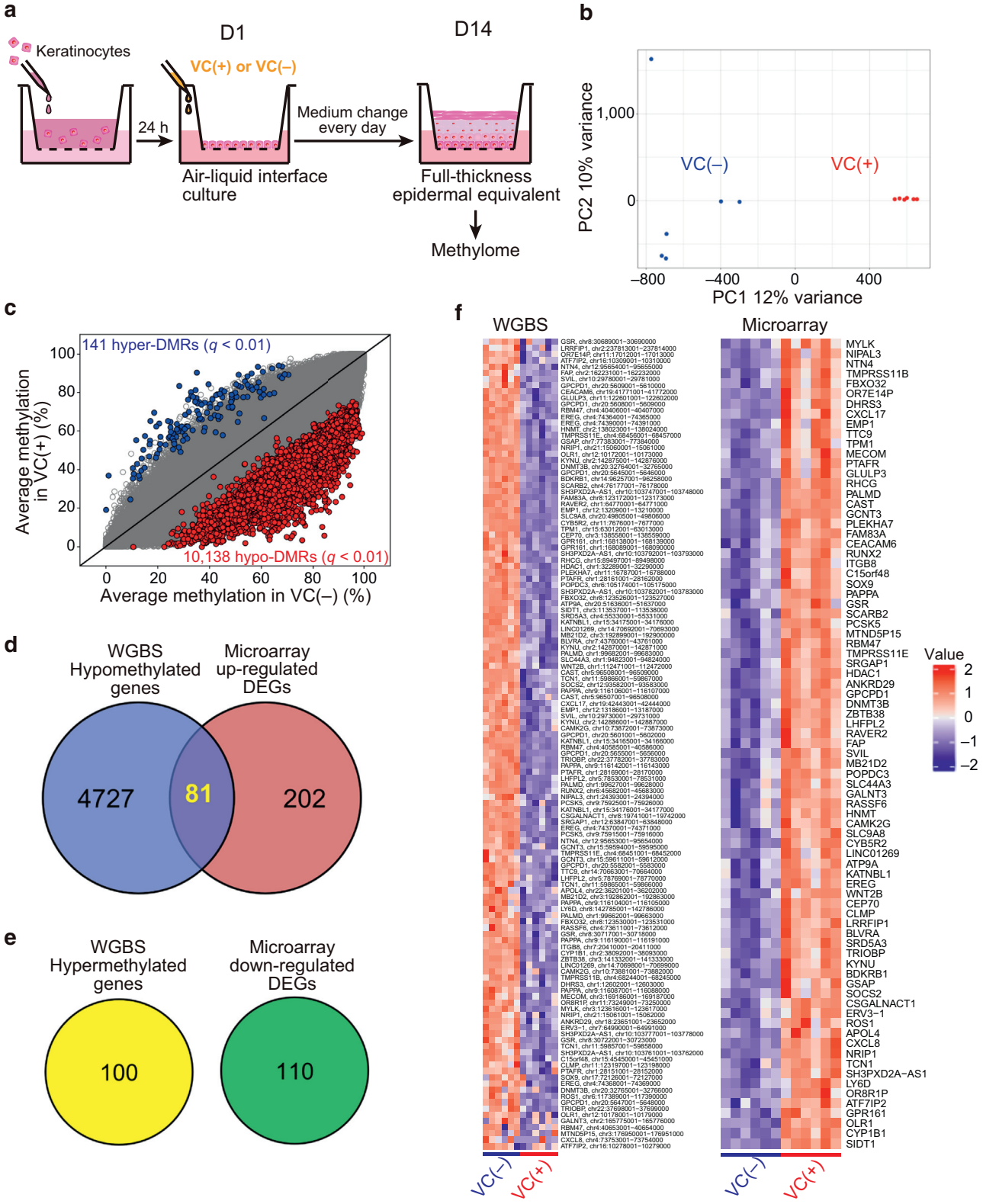

Figure 5. VC increases DNA demethylation profiles. (**a**) Experimental outline for testing the effect of VC on DNA methylation. (**b**) PCA of the DNA methylation profiles identified clear separation between the VC(+) (red) and VC(−) (blue) human epidermal equivalents (n = 6). (**c**) Average methylation per CpG across the VC(+) and VC(−) epidermal models. DMRs were defined by the methylKit logistic regression test and sliding linear model method. The blue and red dots represent 141 hypermethylated DMRs and 10,138 hypomethylated DMRs, respectively. (**d**) Venn diagrams of 4808 hypomethylated genes identified by WGBS and 283 upregulated genes identified by microarray. The numbers of unique and common genes are shown in the Venn diagrams. (**e**) Venn diagrams of 100 hypermethylated genes identified by WGBS and 110 downregulated genes identified by microarray. (**f**) Heatmap showing 81 overlapping genes revealed between the WGBS and the microarray experiments. The left heatmap shows the DMRs in the 81 common genes. The right heatmap shows the DEGs among the 81 overlapping genes. The scale indicates the z score of the methylation rate and microarray signal intensity from lowest (blue) to highest (red) expression. DEG, differentially expressed gene; DMR, differentially methylated region; PCA, principal component analysis; VC, vitamin C; WGBS, whole-genome bisulfite sequencing.

were identified, and the majority (10,138 DMRs) were identified as hypomethylated upon VC treatment (Figure 5c). Given that genes can exhibit multiple DMR patterns, we matched the 10,138 hypomethylated DMRs with 4808 genes and the 141 hypermethylated DMRs with 100 genes. Chromosomal distribution analysis of the DMRs revealed more hypomethylated than hypermethylated DMRs across all chromosomes except the Y chromosome (Supplementary Figure S6b). Examination of the genomic distribution of the DMRs revealed that DNA methylation was maintained in promoter regions, which play pivotal roles for regulating gene expression through DNA methylation (Supplementary Figure S6c). We further analyzed the distribution of DMRs in CpG islands (highly methylated regions located mainly in gene promoters that regulate gene expression by preventing transcription), CpG shore (regions within 2 kb upstream or downstream from a CpG island), and CpG shelf regions (regions between 2 and 4 kb upstream and downstream from a CpG island) (Portela and Esteller, 2010). Although whole-genome DNA demethylation occurred in response to VC treatment, the DNA methylation of the CpG islands was maintained (Supplementary Figure S6d). In contrast, the CpG shore and CpG shelf regions, which are strongly correlated with gene expression through epigenetic modifications (Portela and Esteller, 2010), exhibited DNA demethylation (Supplementary Figure S6d). These results indicate that VC facilitates whole-genome DNA demethylation.

Identification of genes with the potential to affect VC-induced cell proliferation through changes in DNA demethylation

To reveal the cell proliferation–related genes whose regulation VC contributes to through DNA demethylation to induce cell proliferation, we conducted an integrated analysis of the methylome and transcriptome. DNA hypomethylation near gene promoters can lead to increased gene transcription, and hypermethylation near gene promoters can lead to transcriptional silencing (Portela and Esteller, 2010). We analyzed the methylome and transcriptome data and revealed that 81 genes were both hypomethylated and upregulated among 4808 hypomethylated genes and 283 upregulated genes (Figure 5d and Supplementary Table S1). There was no overlap between the 100 hypermethylated genes and the 110 downregulated genes (Figure 5e). Heatmaps made from the WGBS and microarray data revealed clear distinctions in the 81 overlapping genes between the VC-treated and -untreated human epidermal equivalents (Figure 5f and Supplementary Table S1). We further examined the 81 genes to determine whether they had been reported as an epigenetic or epidermal factor and identified 12 genes with the potential to affect VC-induced cell proliferation through changes in DNA demethylation (Supplementary Table S2). DNA methylation was significantly decreased according to WGBS of these 12 genes, and their expression levels were increased according to microarray analysis (Figure 6a and b). We validated the increased expression of these 12 genes in the presence of VC using qPCR analysis and found that all 12 increased by 1.6- to 75.2-fold in the VC-treated human epidermal equivalents (Figure 6c). This result indicates that VC can alleviate gene silencing by promoting DNA demethylation. Collectively, our findings indicate that VC induces the expression of proliferation-related genes by increasing their DNA demethylation, which results in increased epidermal cell proliferation.

DISCUSSION

In this study, we investigated the role of VC in epidermal cell proliferation and differentiation and explored the underlying epigenetic mechanisms in a 3-dimensional cultured human epidermal equivalent model. Studies have shown reduced VC levels in aged or UV-damaged skin (Pullar et al, 2017). Previously, we reported that long-term VC deficiency causes epidermal atrophy in a mouse model with a VC synthesis deficiency (Sato et al, 2012). However, the underlying mechanisms for this had not previously been elucidated. This study demonstrated that intracellular VC uptake by the human epidermal equivalent model increased ECL thickness, cell viability, and cell proliferation. Furthermore, global DNA 5-hmC levels significantly increased in a VC dose-dependent manner. Notably, these effects of VC were attenuated by a TET inhibitor, suggesting that VC promotes keratinocyte proliferation through TET activity. TET activity is catalyzed by a 2-oxoglutarate–dependent iron (II)–containing dioxygenase, and VC is required to reduce iron (III) to iron (II). This study reveals that VC induces DNA demethylation through TETs in a human epidermal equivalent model, clarifying the mechanism through which VC treatment supports skin health and aging.

Profiling transcriptional alterations showed that VC upregulates a DNA replication–related gene set that includes cell proliferation–related genes. A total of 10,138 DMRs were found to be significantly hypomethylated, and 141 DMRs were hypermethylated in the VC-treated group compared with those in the untreated group using the WGBS analysis. These results suggest that VC induced the expression of cell proliferation–related genes through DNA demethylation in the epidermal model.

Interestingly, among the genes found to be both upregulated in expression and hypomethylated upon VC treatment, 12 (*CAST*, *CYP1B1*, *EMP1*, *EREG*, *FAM83A*, *FBXO32*, *HDAC1*, *NTN4*, *RHCG*, *ROS1*, *RUNX2*, and *SOX9*) were previously reported to be associated with cell proliferation (Cai et al, 2020; Chen et al, 2020; Glotzer et al, 2008; Habel et al, 2021; Ichiyama et al, 2015; Iwata et al, 2021; Ji et al, 2021; Kawane et al, 2018; Kumar et al, 2018; Kwon et al, 2016; Li et al, 2015; Lichtenberger et al, 2013; Lin et al, 2015; Lv et al, 2015; Nian and Ma, 2021; Reiners et al, 1998; Schneiders et al, 2007; Shi et al, 2013; Sun et al, 2018; Uchiyama et al, 2019; Yang et al, 2018; Zhang et al, 2021; Zheng et al, 2016; Zhu et al, 2022). The ability of VC to upregulate the mRNA expression of these 12 genes was confirmed through qPCR, and the results showed that *ROS1* was particularly strongly upregulated by VC. ROS1 belongs to the receptor tyrosine kinase family (Azelby et al, 2021). Although the detailed functions of ROS1 are still unclear, receptor tyrosine kinases are known to regulate tissue homeostasis in the normal epidermis (Gurule and Heasley, 2018). In keratinocytes, receptor tyrosine kinases such as EGFRs promote proliferation and delay apoptosis

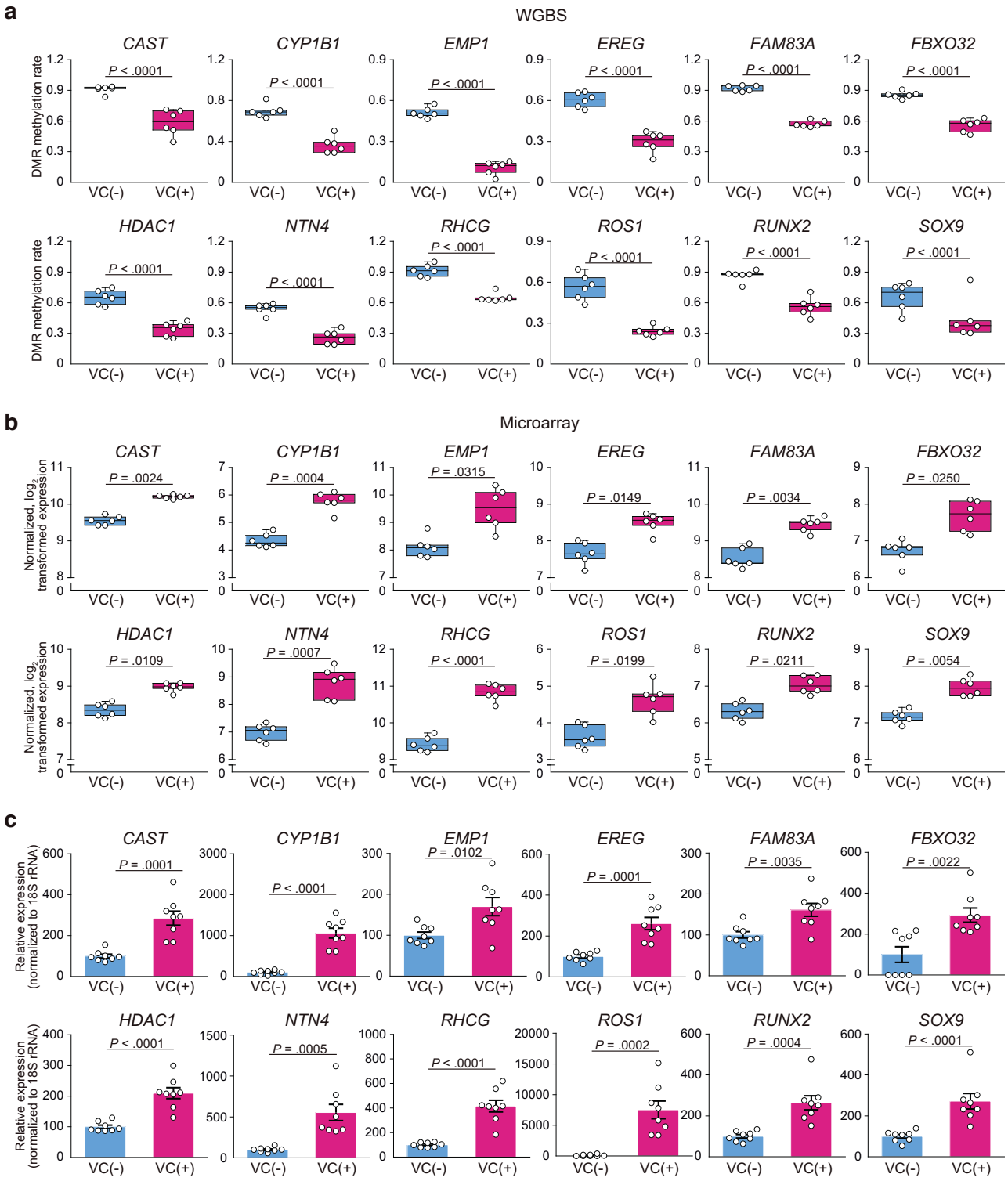

Figure 6. Identification of genes with the potential to affect VC-induced cell proliferation through changes in DNA demethylation. (**a**) The DMR methylation rate (methylation difference ≥25%) of 12 cell proliferation–related genes (n = 6). (**b**) The gene expression levels of 12 cell proliferation–related genes (n = 6). The statistical significance of the DMRs was assessed by the methylKit logistic regression test and sliding linear model method for *P*-value correction. The statistical significance of the gene expression levels was assessed by the Benjamini–Hochberg method for multiple testing calibrations. (**c**) Validation of the expression of 12 cell proliferation–related genes by qPCR (n = 8). Statistical significance was determined by 2-tailed Student's *t*-tests. Source data are provided as a Source Data file. DMR, differentially methylated region; VC, vitamin C.

(Lichtenberger et al, 2013). Therefore, the upregulation of ROS1 might contribute to the VC-induced increase in cell proliferation in the basal layer of the epidermis. However, our gene expression results suggest that not only ROS1 but also multiple other cell proliferation–related genes may act in a complex manner in demethylation-mediated epidermal

thickening induced by VC. The functions of ROS1 and other identified proliferation-related genes should be examined in the future.

VC increases epidermal thickness by promoting keratinocyte proliferation. Epidermal thinning is a known symptom of skin aging (Liu et al, 2019). Recently, epigenetic modifications have been reported to play a role in the regulation of skin homeostasis. Yi et al (2023) reported that 5-hmC levels were decreased in aged human skin. Furthermore, TET2 expression was decreased in keratinocytes treated with hydrogen peroxide, which was followed by an increase in aging-related protein expression (Yi et al, 2023). Moreover, Li et al (2020) observed the loss of 5-hmC in keratinocyte stem cells and transit-amplifying cells in human psoriasis and in imiquimod-induced murine psoriasis. VC-induced restoration of 5-hmC has also been shown to influence downstream genes involved in maintaining epidermal stem cell homeostasis (Li et al, 2020). These reports suggest that decreased DNA demethylation is closely linked to skin aging and disease. Therefore, the DNA demethylation function of VC may contribute to maintaining skin homeostasis, in addition to its other known functions, such as in reducing oxidative stress (Evans and Lawrenson, 2023). In other words, VC deficiency may impair epidermal formation clinically.

Notably, studies have reported that VC induces cell differentiation and reprogramming in several cell types. For example, VC is known to promote the generation of induced pluripotent stem cells (Esteban et al, 2010) and embryonic stem cells (Chung et al, 2010) by reprogramming through epigenetic changes. Kim et al (2018) reported that VC promotes astrocyte differentiation through DNA hydroxymethylation. Furthermore, VC was shown to inhibit proliferation by increasing 5-hmC levels and to promote myeloid differentiation in *TP53*-mutant leukaemia cells (Smith-Díaz et al, 2021). In contrast, this study showed that VC enhanced cell proliferation through TETs in a human epidermal equivalent model. VC has been reported to promote differentiation in keratinocytes (Savini et al, 2002; Pasonen-Seppänen et al, 2001), but our results do not show increased differentiation after exposure to VC. Experimental conditions varied across these studies, including culture methods frequency of VC addition and species in which the experiments were performed. Furthermore, epigenetic effects of VC may differ among tissues and cell types, allowing for variation between reports.

One limitation of the study is that we needed to use VC sodium salt to avoid VC-induced pH changes. Although we demonstrated that sodium alone had no effect on epidermal thickness, cell viability, or DNA demethylation in the human epidermal equivalent model, we cannot exclude the possibility that sodium affects unknown factors. A further limitation of this study is that we did not examine the protein levels of the identified genes because we focused instead on the relationship between epigenetics and gene transcription. Analysis of the protein levels would support the role of proliferation-related factors in the construction of the epidermis. Moreover, VC may alter gene expression through not only DNA methylation changes but also histone modifications and other epigenetic factors (Qin et al, 2023; Thaler et al, 2022). Therefore, further studies are needed to analyze changes in gene expression after TET inhibition and elucidate the potential of VC to rejuvenate the aging epidermis through epigenetic or other modifications.

Collectively, our results suggest that VC is effective at inducing keratinocyte proliferation and epidermal thickening in a human epidermal equivalent model. Epigenetics influence the fate of multiple skin-associated cells in a spatiotemporal manner by affecting the expression and function of target genes. Because epigenetic modifications are reversible, several studies have identified the potential of epigenetic therapies as a tool to reprogram cell fate changes associated with aging. Our study provides insight into possible clinical treatment strategies using VC-mediated epigenetic modifications.

MATERIALS AND METHODS

Construction of human epidermal equivalents

Human epidermal equivalent models were constructed as previously published (Hanada et al, 2014). Normal human epidermal keratinocytes (number 420811D) were purchased from Japan Tissue Engineering (Aichi, Japan). Cryopreserved keratinocytes were thawed and suspended in Assay Medium containing fetal bovine serum (number 402250, Japan Tissue Engineering). Cell aliquots were seeded into 24-well culture inserts (Corning) placed in multiwell culture plates, with each well containing 1.5 ml of culture medium, enough to submerge the keratinocytes, and incubated in a humidified atmosphere of 5% carbon dioxide at 37 °C. After 24 hours of incubation, the medium was removed from the 24-well culture inserts and multiwell culture plates to expose keratinocytes to the air–liquid interface to construct an epidermal equivalent. Freshly prepared medium supplemented with 1.0 mM VC sodium salt (Nacalai Tesque, Kyoto, Japan) was added to only the multiwell culture plates underneath the inserts. For TET inhibitor experiments, 3.75 or 7.50 μM of the TET inhibitor (Bobcat339, Merck) was added to the wells with or without VC. Medium was changed every day, and the human epidermal equivalents were collected after 7 and 14 days.

Histological analysis

Histological analysis was performed as previously published (Kawashima et al, 2018; Sato et al, 2012). Human epidermal equivalents were fixed with a 10% formalin neutral buffer solution (Fujifilm Wako Pure Chemical, Osaka, Japan), embedded in paraffin, and sectioned on a microtome at 5-μm thickness. For H&E staining, the sections were deparaffinized with xylene (Muto Pure Chemicals, Tokyo, Japan), rehydrated with a graded ethanol series (Muto Pure Chemicals), and stained with H&E (Muto Pure Chemicals). To measure the thickness of the ECL and SC, H&E-stained images were acquired using a NanoZoomer 2.0 RS virtual slide scanner (Hamamatsu Photonics, Shizuoka, Japan). The ECL was defined as the distance from the bottom of the basal layer to the top of the granular layer. The thickness of the ECL and SC was measured in 5 randomly selected fields from each section with the measurement tool in NDPview2 viewing software (Hamamatsu Photonics) and averaged.

Immunofluorescence analysis

Immunofluorescence analysis was performed as previously published (Kawashima et al, 2018; Sato et al, 2012). Frozen epidermal sections (5 μm) were fixed with ice-cold acetone (Fujifilm Wako Pure Chemical) for 10 minutes and then blocked with 10% normal goat serum (Funakoshi, Tokyo, Japan) in PBS without calcium and magnesium (PBS [−]) for 1 hour at room temperature. Sections were

then incubated with primary antibodies (rabbit anti-K10 [1:1,000; BioLegend, number 905404], rabbit antiloricrin [1:500; BioLegend, number 905104], mouse anti-K14 [1:200; Abcam, Cambridge, United Kingdom, number ab7800], rabbit anti-FLG [1:5000] [Senshu et al, 1995], rabbit anti-K1 [1:2500] [Senshu et al, 1996], rabbit anti−5-hmC [1:500; Active Motif, number 39769], mouse anti−5-mC [1:200; Active Motif, number 91187], and rabbit anti−Ki-67 [1:400; Cell Signaling Technology, number 12202]) diluted with PBS (−) containing 0.1% Tween-20 (Fujifilm Wako Pure Chemical) at 4 °C overnight. Sections were then incubated with secondary antibodies (Alexa Fluor 488−conjugated goat antirabbit IgG [1:2500; Thermo Fisher Scientific, number A11070] and goat antimouse IgG [1:2500; Thermo Fisher Scientific, number A11017]) diluted in PBS (−) containing 0.1% Tween-20 and 1% BSA (Fujifilm Wako Pure Chemical) at 4 °C for 2 hours. Between solution changes, all sections were washed 3 times with PBS (−) for 5 minutes each. Nuclei were stained with a DAPI (Bio-Rad Laboratories) solution for 15 minutes at room temperature and mounted with Fluoromount/Plus (Cosmo Bio, Tokyo, Japan) prior to fluorescence detection of 5-mC, 5-hmC, and Ki-67. Fluorescent signals were detected with an Axio Vert.A1 instrument (Carl Zeiss, Hallbergmoos, Germany). The number of Ki-67−, 5-mC−, and 5-hmC−positive cells (signal intensity exceeding the threshold of detection in each nucleus) were counted in randomly selected field from each section.

Measurement of VC concentrations

VC concentrations in the epidermal equivalent and culture medium were measured using high-performance liquid chromatography and electrochemical detection, as previously described (Sato et al, 2010). After 7 and 14 days of culture, human epidermal equivalents were washed with ice-cold PBS (−) and homogenized using a handy homogenizer (PT-33M; Nippon Genetics, Tokyo, Japan) with 0.1% SDS. An equal amount of 10% metaphosphoric acid containing 1 mM EDTA was added to the homogenized samples. The culture medium (100 μl) was collected 0, 1, 3, 6, 12, and 24 hours after addition of VC and mixed with an equal amount of 10% metaphosphoric acid containing 1 mM EDTA. After centrifugation at 21,000*g* for 10 minutes at 4 °C, the concentrations of the L-ascorbic acid and dehydroascorbic acid forms of VC in the centrifugal supernatants were measured and normalized to the protein concentration, which was quantified using a Pierce BCA protein assay kit, following the manufacturer's instructions (Thermo Fisher Scientific).

Measurement of cell viability

The cell viability of the epidermal equivalents was evaluated using a 3-(4,5-dimethylthiazol-2-yl)-2,5-diphenyltetrazolium bromide (Nacalai Tesque) viability assay. Each of the epidermal equivalents was washed with PBS (−) and incubated with freshly prepared culture medium supplemented with the 3-(4,5-dimethylthiazol-2-yl)-2,5-diphenyltetrazolium bromide solution (0.5 mg/ml), as per the assay instructions, for 3 hours at 37 °C in a carbon dioxide incubator. A whole sample of each epidermal equivalent was removed with a scalpel, immersed in 300 μl of 2-isopropanol (Nacalai Tesque), and incubated for 15 hours at 37 °C to completely extract the formazan product. Subsequently, 200 μl of each extract was transferred to a 96-well microplate, and the absorbance at 570 and 650 nm as a reference was measured using a microplate reader. The absorbance of the extract from untreated tissues was set as 100%. The cell viability of the tissues was expressed as the percentage compared with that of the control tissue.

Dot blot analysis

DNA was extracted with a QIAamp DNA Micro Kit (Qiagen, Hilden, Germany), according to the manufacturer's instructions. The DNA concentration was determined with a NanoDrop One spectrophotometer (Thermo Fisher Scientific). After dilution with TE buffer (10 mM Tris-hydrogen chloride, 1 mM EDTA), the DNA samples were denatured with 1 volume of DNA denaturing buffer (200 mM sodium hydroxide, 20 mM EDTA) for 10 minutes at 95 °C, neutralized with 2 volumes of 20× saline-sodium citrate buffer (Nippon Gene), and chilled on ice for 5 minutes. The DNA samples were spotted on a positively charged nylon membrane (Amersham Hybond-N^+; Cytiva, Tokyo, Japan) using a Bio-Dot Apparatus (Bio-Rad Laboratories) and cross-linked by a UV crosslinker at 120 mJ/cm^2 (Cosmo Bio). The membrane was blocked with 5% skim milk/Tris-buffered saline containing 0.1% Tween-20 (Fujifilm Wako Pure Chemical) for 1 hour at room temperature and incubated with rabbit anti−5-hmC (1:10,000; Active Motif, number 39769) or mouse anti−5-mC (1:1000; Active Motif, number 91187) overnight at 4 °C. After washing 3 times with Tris-buffered saline containing 0.1% Tween-20, the membrane was incubated with an antirabbit (1:2500; Promega, number W4011) or antimouse (1:2500; Promega, number W4021) IgG secondary antibody for 1 hour at room temperature. Chemiluminescence signals were detected with a Fusion Solo.7-S.Edge instrument (M&S Instruments, Osaka, Japan) using an enhanced chemiluminescence western blotting analysis system (Cytiva) and quantified with Multi Gauge V3.0 software (Fujifilm, Tokyo, Japan).

Microarray and data analysis

Total RNA was extracted from a half portion of human epidermal equivalents grown with or without 1.0 mM VC for 14 days using an miRNeasy Mini Kit (Qiagen), according to the manufacturer's instructions. The integrity and quality of the RNA were evaluated using a NanoDrop One and Agilent 2100 Bioanalyzer (Agilent Technologies) prior to analysis. Labeled cDNA samples were prepared from total RNA using a GeneChip WT PLUS Reagent Kit (Thermo Fisher Scientific), according to the manufacturer's instructions, and then hybridized to human Clariom D microarrays (Thermo Fisher Scientific). The arrays were scanned on a GeneChip Scanner 3000 7G instrument (Thermo Fisher Scientific), and the data were analyzed using Affymetrix GeneChip Command Console software (version 4.0). Raw data were normalized by SST-RMA (signal space transformation robust multichip analysis) algorithm, and quality checks such as labeling and hybridization were performed using Transcriptome Analysis Console 4.0 software (Thermo Fisher Scientific). Principal component analysis, hierarchical cluster analysis, and the generation of scatter plots and volcano plots were carried out using Transcriptome Analysis Console 4.0 software. Gene set enrichment analysis was performed using gene set enrichment analysis software, version 4.1.0 (Subramanian et al, 2005).

WGBS and data analysis

Genomic DNA was extracted from a half portion of human epidermal equivalents using the Monarch Genomic DNA Purification Kit (New England Biolabs, Ipswich, MA). The integrity and quality of the DNA were evaluated using a NanoDrop One and TapeStation (Agilent Technologies) prior to analysis. DNA methylation sequencing was performed, and the data were analyzed using a previously described WGBS methodology (Lister et al, 2009). Bisulfite treatment was performed using a Swift Biosciences Accel-NGS Methyl-Seq DNA Library Kit (Swift Biosciences, Ann Arbor,

MI) to generate WGBS libraries. The amplified libraries were sequenced using an Illumina Nova Seq 6000 with 150 bp paired-end reads, following standard Illumina sequencing protocols. To analyze the bisulfite sequencing results, the quality of the raw paired-end sequence reads was assessed with FastQC (version 0.11.7). Low-quality (<20 bases) or 5′-end 10-base sequences and adapter sequences were trimmed by Trim Galore (version 0.5.0) with the options "-q 20 –phred33 –clip_R1 10 –clip_R2 10 —paired." The trimmed reads were aligned to the reference genome using methylpy (version 1.4.6) with the options "–remove-clonal True –trim-reads FALSE." Annotation was performed with in-house software. The number of methylated cytosines in the 1000 bases of nonoverlapping windows across the whole genome was estimated by the tileMethylCounts function from the methylKit (version 1.10.0) package (Akalin et al, 2012). Normalization was performed using the normalizeCoverage function in methylKit. Bases with less than 10× read coverage and bases with more than 99.9th percentile coverage in each sample (likely PCR artifacts with abnormally high coverage) were removed by the filterByCoverage function of methylKit. All samples were then merged using the unite function in methylKit with the destrand = FALSE option. To identify DMRs, differential methylation was calculated using the calculate DiffMeth function of methylKit. Regions with a q-value <0.01 and a methylation change >25% between the groups were considered significant DMRs. A cluster analysis heatmap of the DMRs and differentially expressed genes was generated with ComplexHeatmap (version 2.12.1). To perform an integrated analysis of the gene expression and DNA methylation profiles, normalization of the gene expression levels was performed using the robust multiarray average method with oligo software, and the expression levels were corrected among the samples. The program limma (Bioconductor) was used for comparisons between the groups.

RT-qPCR

Total RNA was extracted from a half portion of human epidermal equivalents using QIAzol lysis reagent (Qiagen) or ISOGEN (Nippon Gene) and processed through a RNeasy Mini spin column (Qiagen), according to the manufacturer's instructions. RNA concentrations were quantified with a NanoDrop spectrophotometer. cDNA was synthesized from RNA using SuperScript III reverse transcriptase (Thermo Fisher Scientific), according to the manufacturer's instructions. RT-PCR was performed using the QuantStudio 3 system (Thermo Fisher Scientific) and THUNDERBIRD SYBR qPCR Mix (Toyobo, Osaka, Japan), according to the manufacturers' instructions. Primers (sequences shown in Supplementary Table S3) were purchased from Eurofins Genomics Japan (Tokyo, Japan). The amplification protocol consisted of denaturation at 95 °C for 1 minute, followed by 40 cycles of 95 °C for 15 seconds and 60 °C for 1 minutes. Gene expression levels were normalized to 18S ribosomal RNA.

Statistical analysis

Statistical analysis was performed with KaleidaGraph software (version 5.0; Synergy Software). Comparisons of multiple groups were performed using 1-way ANOVA followed by Tukey's or Dunnett's posthoc tests. Pairwise comparisons between 2 groups were performed using an unpaired 2-tailed Student's *t*-test. Details of each statistical test used are specified in the figure legends. Statistical significance was defined at $P < .05$. Error bars in the figures indicate the SD or SEM from the replicates, as indicated in the figure legends.

DATA AVAILABILITY STATEMENT

Microarray and whole-genome bisulfite sequencing datasets generated and analyzed during this study are deposited in the Gene Expression Omnibus under accession codes GSE274382 (https://www.ncbi.nlm.nih.gov/geo/query/acc.cgi?acc=GSE274382) and GSE273778 (https://www.ncbi.nlm.nih.gov/geo/query/acc.cgi?acc=GSE273778), respectively. All other data generated in this study are provided in supplementary materials and provided in the Source Data file associated with this paper.

ORCIDs

Yasunori Sato: http://orcid.org/0009-0000-9550-4866
Ayami Sato: http://orcid.org/0000-0002-7715-2112
Florence: http://orcid.org/0009-0006-8978-894X
Akari Kuwano: http://orcid.org/0009-0007-7935-2648
Yasunari Sato: http://orcid.org/0000-0003-2173-8488
Hideki Tanaka: http://orcid.org/0009-0001-9736-1683
Toshiyuki Kimura: http://orcid.org/0000-0003-0006-7355
Tsuyoshi Ishii: http://orcid.org/0000-0001-9174-2744
Akihito Ishigami: http://orcid.org/0000-0001-7875-7482

CONFLICT OF INTEREST

F, AK, YS, and TI are employed by ROHTO Pharmaceutical. The remaining authors state no conflict of interest.

ACKNOWLEDGMENTS

We thank Y. Takino, S. Kochi, H. Kaneko, and members of the Kimura laboratory at Hokuriku University for their technical assistance. This study was supported by grants from the Japan Society for the Promotion of Science KAKENHI (grant number 19K05902 [YS]). We thank DerMEDit for language editing and scientific advice in preparation of this manuscript. This study was exempt from Institutional Review Board review because all the data consisted of commercially available human biological specimens.

AUTHOR CONTRIBUTIONS

Conceptualization: YS, AS, F, AK, YS, HT, TK, TI, AI; Data Curation: YS, AS, F, AK, YS, HT, TK, TI, AI; Formal Analysis: YS, AS, F, AK, YS, HT, TK, TI, AI; Investigation: YS, AS, F, AK, YS, HT, TK, TI, AI; Methodology: YS, AS, F, AK, YS, HT, TK, TI, AI; Project Administration: YS, AS, F, AK, YS, HT, TK, TI, AI; Resources: YS, AS, F, AK, YS, HT, TK, TI, AI; Validation: YS, AS, F, AK, YS, HT, TK, TI, AI; Visualization: YS, AS, F, AK, YS, HT, TK, TI, AI; Writing - Original Draft Preparation: YS, AS, F, AK, YS, HT, TK, TI, AI; Writing - Review and Editing: YS, AS, F, AK, YS, HT, TK, TI, AI

SUPPLEMENTARY MATERIAL

Supplementary material is linked to the online version of the paper at www.jidonline.org, and at https://doi.org/10.1016/j.jid.2025.03.040.

REFERENCES

Akalin A, Kormaksson M, Li S, Garrett-Bakelman FE, Figueroa ME, Melnick A, et al. MethylKit: a comprehensive R package for the analysis of genome-wide DNA methylation profiles. Genome Biol 2012;13:R87.

Azelby CM, Sakamoto MR, Bowles DW. ROS1 targeted therapies: current status. Curr Oncol Rep 2021;23:94.

Blaschke K, Ebata KT, Karimi MM, Zepeda-Martínez JA, Goyal P, Mahapatra S, et al. Vitamin C induces Tet-dependent DNA demethylation and a blastocyst-like state in ES cells. Nature 2013;500:222—6.

Boyce ST, Supp AP, Swope VB, Warden GD. Vitamin C regulates keratinocyte viability, epidermal barrier, and basement membrane in vitro, and reduces wound contraction after grafting of cultured skin substitutes. J Invest Dermatol 2002;118:565—72.

Cai EY, Kufeld MN, Schuster S, Arora S, Larkin M, Germanos AA, et al. Selective translation of cell fate regulators mediates tolerance to broad oncogenic stress. Cell Stem Cell 2020;27:270—83.e7.

Chen P, Liu C, Li P, Wang Q, Gao X, Wu H, et al. High RhCG expression predicts poor survival and promotes migration and proliferation of gastric cancer via keeping intracellular alkaline. Exp Cell Res 2020;386:111740.

Choi EH. Aging of the skin barrier. Clin Dermatol 2019;37:336—45.

Chung TL, Brena RM, Kolle G, Grimmond SM, Berman BP, Laird PW, et al. Vitamin C promotes widespread yet specific DNA demethylation of the epigenome in human embryonic stem cells. Stem Cells 2010;28:1848—55.

Cimmino L, Dolgalev I, Wang Y, Yoshimi A, Martin GH, Wang J, et al. Restoration of TET2 function blocks aberrant self-renewal and leukemia progression. Cell 2017;170:1079—95.e20.

DiTroia SP, Percharde M, Guerquin MJ, Wall E, Collignon E, Ebata KT, et al. Maternal vitamin C regulates reprogramming of DNA methylation and germline development. Nature 2019;573:271–5.

Eckhart L, Lippens S, Tschachler E, Declercq W. Cell death by cornification. Biochim Biophys Acta 2013;1833:3471–80.

Esteban MA, Wang T, Qin B, Yang J, Qin D, Cai J, et al. Vitamin C enhances the generation of mouse and human induced pluripotent stem cells. Cell Stem Cell 2010;6:71–9.

Evans JR, Lawrenson JG. Antioxidant vitamin and mineral supplements for slowing the progression of age-related macular degeneration. Cochrane Database Syst Rev 2023;9:CD000254.

Glotzer DJ, Zelzer E, Olsen BR. Impaired skin and hair follicle development in Runx2 deficient mice. Dev Biol 2008;315:459–73.

Gurule NJ, Heasley LE. Linking tyrosine kinase inhibitor-mediated inflammation with normal epithelial cell homeostasis and tumor therapeutic responses. Cancer Drug Resist 2018;1:118–25.

Habel N, El-Hachem N, Soysouvanh F, Hadhiri-Bzioueche H, Giuliano S, Nguyen S, et al. FBXO32 links ubiquitination to epigenetic reprograming of melanoma cells. Cell Death Differ 2021;28:1837–48.

Hanada T, Itahara Y, Katoh M, Inoie M, Hata K. Keratinization induced by air exposure in the reconstructed human epidermal model: an in vitro model of a cultured epithelial autograft. J Biosci Bioeng 2014;118:323–6.

Henry J, Toulza E, Hsu CY, Pellerin L, Balica S, Mazereeuw-Hautier J, et al. Update on the epidermal differentiation complex. Front Biosci (Landmark Ed) 2012;17:1517–32.

Ichiyama K, Chen T, Wang X, Yan X, Kim BS, Tanaka S, et al. The methylcytosine dioxygenase Tet2 promotes DNA demethylation and activation of cytokine gene expression in T cells. Immunity 2015;42:613–26.

Iwata H, Haga N, Ujiie H. Possible role of epiregulin from dermal fibroblasts in the keratinocyte hyperproliferation of psoriasis. J Dermatol 2021;48:1433–8.

Ji H, Song H, Wang Z, Jiao P, Xu J, Li X, et al. FAM83A promotes proliferation and metastasis via Wnt/β-catenin signaling in head neck squamous cell carcinoma. J Transl Med 2021;19:423.

Kawane T, Qin X, Jiang Q, Miyazaki T, Komori H, Yoshida CA, et al. Runx2 is required for the proliferation of osteoblast progenitors and induces proliferation by regulating Fgfr2 and FGFR3. Sci Rep 2018;8:13551.

Kawashima S, Funakoshi T, Sato Y, Saito N, Ohsawa H, Kurita K, et al. Protective effect of pre- and post-vitamin C treatments on UVB-irradiation-induced skin damage. Sci Rep 2018;8:16199.

Kim JH, Kim M, He XB, Wulansari N, Yoon BH, Bae DH, et al. Vitamin C promotes astrocyte differentiation through DNA hydroxymethylation. Stem Cells 2018;36:1578–88.

Kishimoto Y, Saito N, Kurita K, Shimokado K, Maruyama N, Ishigami A. Ascorbic acid enhances the expression of type 1 and type 4 collagen and SVCT2 in cultured human skin fibroblasts. Biochem Biophys Res Commun 2013;430:579–84.

Kumar S, Chinnusamy V, Mohapatra T. Epigenetics of modified DNA bases: 5-methylcytosine and beyond. Front Genet 2018;9:640.

Kwon YJ, Baek HS, Ye DJ, Shin S, Kim D, Chun YJ. CYP1B1 enhances cell proliferation and metastasis through induction of EMT and activation of wnt/β-catenin signaling via Sp1 upregulation. PLoS One 2016;11:e0151598.

Lee Chong T, Ahearn EL, Cimmino L. Reprogramming the epigenome with vitamin C. Front Cell Dev Biol 2019;7:128.

Li D, Li XI, Wang A, Meisgen F, Pivarcsi A, Sonkoly E, et al. MicroRNA-31 promotes skin wound healing by enhancing keratinocyte proliferation and migration. J Invest Dermatol 2015;135:1676–85.

Li F, Yuan CW, Xu S, Zu T, Woappi Y, Lee CAA, et al. Loss of the epigenetic Mark 5-hmC in psoriasis: implications for epidermal stem cell dysregulation. J Invest Dermatol 2020;140:1266–75.e3.

Lichtenberger BM, Gerber PA, Holcmann M, Buhren BA, Amberg N, Smolle V, et al. Epidermal EGFR controls cutaneous host defense and prevents inflammation. Sci Transl Med 2013;5:199ra111.

Lin JR, Qin HH, Wu WY, He SJ, Xu JH. Vitamin C protects against UV irradiation-induced apoptosis through reactivating silenced tumor suppressor genes p21 and p16 in a Tet-dependent DNA demethylation manner in human skin cancer cells. Cancer Biother Radiopharm 2014;29:257–64.

Lin Z, Zhao J, Nitoiu D, Scott CA, Plagnol V, Smith FJ, et al. Loss-of-function mutations in CAST cause peeling skin, leukonychia, acral punctate keratoses, cheilitis, and knuckle pads. Am J Hum Genet 2015;96:440–7.

Lister R, Pelizzola M, Dowen RH, Hawkins RD, Hon G, Tonti-Filippini J, et al. Human DNA methylomes at base resolution show widespread epigenomic differences. Nature 2009;462:315–22.

Liu N, Matsumura H, Kato T, Ichinose S, Takada A, Namiki T, et al. Stem cell competition orchestrates skin homeostasis and ageing. Nature 2019;568:344–50.

Lv B, Song C, Wu L, Zhang Q, Hou D, Chen P, et al. Netrin-4 as a biomarker promotes cell proliferation and invasion in gastric cancer. Oncotarget 2015;6:9794–806.

Masaki H. Role of antioxidants in the skin: anti-aging effects. J Dermatol Sci 2010;58:85–90.

Michalak M, Pierzak M, Kręcisz B, Suliga E. Bioactive compounds for skin health: a review. Nutrients 2021;13:203.

Minor EA, Court BL, Young JI, Wang G. Ascorbate induces ten-eleven translocation (Tet) methylcytosine dioxygenase-mediated generation of 5-hydroxymethylcytosine. J Biol Chem 2013;288:13669–74.

Morizane S, Mukai T, Sunagawa K, Tachibana K, Kawakami Y, Ouchida M. "Input/output cytokines" in epidermal keratinocytes and the involvement in inflammatory skin diseases. Front Immunol 2023;14:1239598.

Mulder KW, Wang X, Escriu C, Ito Y, Schwarz RF, Gillis J, et al. Diverse epigenetic strategies interact to control epidermal differentiation. Nat Cell Biol 2012;14:753–63.

Nian H, Ma B. Calpain-calpastatin system and cancer progression. Biol Rev Camb Philos Soc 2021;96:961–75.

Padayatty SJ, Sun H, Wang Y, Riordan HD, Hewitt SM, Katz A, et al. Vitamin C pharmacokinetics: implications for oral and intravenous use. Ann Intern Med 2004;140:533–7.

Pasonen-Seppänen S, Suhonen TM, Kirjavainen M, Suihko E, Urtti A, Miettinen M, et al. Vitamin C enhances differentiation of a continuous keratinocyte cell line (REK) into epidermis with normal stratum corneum ultrastructure and functional permeability barrier. Histochem Cell Biol 2001;116:287–97.

Portela A, Esteller M. Epigenetic modifications and human disease. Nat Biotechnol 2010;28:1057–68.

Pullar JM, Carr AC, Vissers MCM. The roles of vitamin C in skin health. Nutrients 2017;9:866.

Qin S, Wang G, Chen L, Geng H, Zheng Y, Xia C, et al. Pharmacological vitamin C inhibits mTOR signaling and tumor growth by degrading Rictor and inducing HMOX1 expression. PLoS Genet 2023;19:e1010629.

Ramos-e-Silva M, Jacques Cd. Epidermal barrier function and systemic diseases. Clin Dermatol 2012;30:277–9.

Reiners JJ Jr, Jones CL, Hong N, Myrand SP. Differential induction of Cyp1a1, Cyp1b1, Ahd4, and Nmo1 in murine skin tumors and adjacent normal epidermis by ligands of the aryl hydrocarbon receptor. Mol Carcinog 1998;21:135–46.

Richelle M, Sabatier M, Steiling H, Williamson G. Skin bioavailability of dietary vitamin E, carotenoids, polyphenols, vitamin C, zinc and selenium. Br J Nutr 2006;96:227–38.

Sajadian SO, Tripura C, Samani FS, Ruoss M, Dooley S, Baharvand H, et al. Vitamin C enhances epigenetic modifications induced by 5-azacytidine and cell cycle arrest in the hepatocellular carcinoma cell lines HLE and Huh7. Clin Epigenetics 2016;8:46.

Sato Y, Arai KY, Nishiyama T, Nomura Y, Kishimoto Y, Aizawa S, et al. Ascorbic acid deficiency leads to epidermal atrophy and UVB-induced skin pigmentation in SMP30/GNL knockout hairless mice. J Invest Dermatol 2012;132:2112–5.

Sato Y, Uchida E, Aoki H, Hanamura T, Nagamine K, Kato H, et al. Acerola (*Malpighia emarginata* DC.) juice intake suppresses UVB-induced skin pigmentation in SMP30/GNL knockout hairless mice. PLoS One 2017;12:e0170438.

Sato Y, Uchiki T, Iwama M, Kishimoto Y, Takahashi R, Ishigami A. Determination of dehydroascorbic acid in mouse tissues and plasma by using tris(2-carboxyethyl)phosphine hydrochloride as reductant in metaphosphoric acid/ethylenediaminetetraacetic acid solution. Biol Pharm Bull 2010;33:364–9.

Savini I, Catani MV, Rossi A, Duranti G, Melino G, Avigliano L. Characterization of keratinocyte differentiation induced by ascorbic acid: protein kinase C involvement and vitamin C homeostasis. J Invest Dermatol 2002;118:372–9.

Schneiders FI, Maertens B, Böse K, Li Y, Brunken WJ, Paulsson M, et al. Binding of netrin-4 to laminin short arms regulates basement membrane assembly. J Biol Chem 2007;282:23750–8.

Senshu T, Akiyama K, Kan S, Asaga H, Ishigami A, Manabe M. Detection of deiminated proteins in rat skin: probing with a monospecific antibody after modification of citrulline residues. J Invest Dermatol 1995;105:163–9.

Senshu T, Kan S, Ogawa H, Manabe M, Asaga H. Preferential deimination of keratin K1 and filaggrin during the terminal differentiation of human epidermis. Biochem Biophys Res Commun 1996;225:712–9.

Shenoy N, Bhagat T, Nieves E, Stenson M, Lawson J, Choudhary GS, et al. Upregulation of TET activity with ascorbic acid induces epigenetic modulation of lymphoma cells. Blood Cancer J 2017;7:e587.

Shi G, Sohn KC, Li Z, Choi DK, Park YM, Kim JH, et al. Expression and functional role of Sox9 in human epidermal keratinocytes. PLoS One 2013;8:e54355.

Smith-Díaz CC, Magon NJ, McKenzie JL, Hampton MB, Vissers MCM, Das AB. Ascorbate inhibits proliferation and promotes myeloid differentiation in TP53-mutant leukemia. Front Oncol 2021;11:709543.

Subramanian A, Tamayo P, Mootha VK, Mukherjee S, Ebert BL, Gillette MA, et al. Gene set enrichment analysis: a knowledge-based approach for interpreting genome-wide expression profiles. Proc Natl Acad Sci USA 2005;102:15545–50.

Sun J, He X, Zhu Y, Ding Z, Dong H, Feng Y, et al. SIRT1 activation disrupts maintenance of myelodysplastic syndrome stem and progenitor cells by restoring TET2 function. Cell Stem Cell 2018;23:355–69.e9.

Thaler R, Khani F, Sturmlechner I, Dehghani SS, Denbeigh JM, Zhou X, et al. Vitamin C epigenetically controls osteogenesis and bone mineralization. Nat Commun 2022;13:5883.

Uchiyama A, Nayak S, Graf R, Cross M, Hasneen K, Gutkind JS, et al. SOX2 epidermal overexpression promotes cutaneous wound healing via activation of EGFR/MEK/ERK signaling mediated by EGFR ligands. J Invest Dermatol 2019;139:1809–20.e8.

Yang R, Yu T, Kou X, Gao X, Chen C, Liu D, et al. Tet1 and Tet2 maintain mesenchymal stem cell homeostasis via demethylation of the P2rX7 promoter. Nat Commun 2018;9:2143.

Yi Y, Wang Y, Wu Y, Liu Y. Targeting SIRT4/TET2 signaling alleviates human keratinocyte senescence by reducing 5-hydroxymethylcytosine loss. Lab Invest 2023:100268.

Young JI, Züchner S, Wang G. Regulation of the epigenome by vitamin C. Annu Rev Nutr 2015;35:545–64.

Zhang H, Weström S, Kappelin P, Virtanen M, Vahlquist A, Törmä H. Exploration of novel candidate genes involved in epidermal keratinocyte differentiation and skin barrier repair in man. Differentiation 2021;119:19–27.

Zheng L, Zhai Y, Li N, Ma F, Zhu H, Du X, et al. The modification of Tet1 in male germline stem cells and interact with PCNA, HDAC1 to promote their self-renewal and proliferation. Sci Rep 2016;6:37414.

Zhu X, Leboeuf M, Liu F, Grachtchouk M, Seykora JT, Morrisey EE, et al. HDAC1/2 control proliferation and survival in adult epidermis and pre–basal cell carcinoma through p16 and p53. J Invest Dermatol 2022;142:77–87.e10.

SUPPLEMENTARY REFERENCES

Cai EY, Kufeld MN, Schuster S, Arora S, Larkin M, Germanos AA, et al. Selective translation of cell fate regulators mediates tolerance to broad oncogenic stress. Cell Stem Cell 2020;27:270–83.e7.

Chen P, Liu C, Li P, Wang Q, Gao X, Wu H, et al. High RhCG expression predicts poor survival and promotes migration and proliferation of gastric cancer via keeping intracellular alkaline. Exp Cell Res 2020;386:111740.

Glotzer DJ, Zelzer E, Olsen BR. Impaired skin and hair follicle development in Runx2 deficient mice. Dev Biol 2008;315:459–73.

Habel N, El-Hachem N, Soysouvanh F, Hadhiri-Bzioueche H, Giuliano S, Nguyen S, et al. FBXO32 links ubiquitination to epigenetic reprograming of melanoma cells. Cell Death Differ 2021;28:1837–48.

Ichiyama K, Chen T, Wang X, Yan X, Kim BS, Tanaka S, et al. The methylcytosine dioxygenase Tet2 promotes DNA demethylation and activation of cytokine gene expression in T cells. Immunity 2015;42:613–26.

Iwata H, Haga N, Ujiie H. Possible role of epiregulin from dermal fibroblasts in the keratinocyte hyperproliferation of psoriasis. J Dermatol 2021;48:1433–8.

Ji H, Song H, Wang Z, Jiao P, Xu J, Li X, et al. FAM83A promotes proliferation and metastasis via Wnt/β-catenin signaling in head neck squamous cell carcinoma. J Transl Med 2021;19:423.

Kawane T, Qin X, Jiang Q, Miyazaki T, Komori H, Yoshida CA, et al. Runx2 is required for the proliferation of osteoblast progenitors and induces proliferation by regulating Fgfr2 and FGFR3. Sci Rep 2018;8:13551.

Kumar S, Chinnusamy V, Mohapatra T. Epigenetics of modified DNA bases: 5-methylcytosine and beyond. Front Genet 2018;9:640.

Kwon YJ, Baek HS, Ye DJ, Shin S, Kim D, Chun YJ. CYP1B1 enhances cell proliferation and metastasis through induction of EMT and activation of Wnt/β-catenin signaling via Sp1 upregulation. PLoS One 2016;11:e0151598.

Li D, Li XI, Wang A, Meisgen F, Pivarcsi A, Sonkoly E, et al. MicroRNA-31 promotes skin wound healing by enhancing keratinocyte proliferation and migration. J Invest Dermatol 2015;135:1676–85.

Lichtenberger BM, Gerber PA, Holcmann M, Buhren BA, Amberg N, Smolle V, et al. Epidermal EGFR controls cutaneous host defense and prevents inflammation. Sci Transl Med 2013;5:199ra111.

Lin Z, Zhao J, Nitoiu D, Scott CA, Plagnol V, Smith FJ, et al. Loss-of-function mutations in CAST cause peeling skin, leukonychia, acral punctate keratoses, cheilitis, and knuckle pads. Am J Hum Genet 2015;96:440–7.

Lv B, Song C, Wu L, Zhang Q, Hou D, Chen P, et al. Netrin-4 as a biomarker promotes cell proliferation and invasion in gastric cancer. Oncotarget 2015;6:9794–806.

Nian H, Ma B. Calpain-calpastatin system and cancer progression. Biol Rev Camb Philos Soc 2021;96:961–75.

Reiners JJ Jr, Jones CL, Hong N, Myrand SP. Differential induction of Cyp1a1, Cyp1b1, Ahd4, and Nmo1 in murine skin tumors and adjacent normal epidermis by ligands of the aryl hydrocarbon receptor. Mol Carcinog 1998;21:135–46.

Schneiders FI, Maertens B, Böse K, Li Y, Brunken WJ, Paulsson M, et al. Binding of netrin-4 to laminin short arms regulates basement membrane assembly. J Biol Chem 2007;282:23750–8.

Shi G, Sohn KC, Li Z, Choi DK, Park YM, Kim JH, et al. Expression and functional role of Sox9 in human epidermal keratinocytes. PLoS One 2013;8:e54355.

Sun J, He X, Zhu Y, Ding Z, Dong H, Feng Y, et al. SIRT1 Activation disrupts maintenance of myelodysplastic syndrome stem and progenitor cells by restoring TET2 function. Cell Stem Cell 2018;23:355–69.e9.

Uchiyama A, Nayak S, Graf R, Cross M, Hasneen K, Gutkind JS, et al. SOX2 epidermal overexpression promotes cutaneous wound healing via activation of EGFR/MEK/ERK signaling mediated by EGFR ligands. J Invest Dermatol 2019;139:1809–20.e8.

Yang R, Yu T, Kou X, Gao X, Chen C, Liu D, et al. Tet1 and Tet2 maintain mesenchymal stem cell homeostasis via demethylation of the P2rX7 promoter. Nat Commun 2018;9:2143.

Zhang H, Weström S, Kappelin P, Virtanen M, Vahlquist A, Törmä H. Exploration of novel candidate genes involved in epidermal keratinocyte differentiation and skin barrier repair in man. Differentiation 2021;119:19–27.

Zheng L, Zhai Y, Li N, Ma F, Zhu H, Du X, et al. The modification of Tet1 in male germline stem cells and interact with PCNA, HDAC1 to promote their self-renewal and proliferation. Sci Rep 2016;6:37414.

Zhu X, Leboeuf M, Liu F, Grachtchouk M, Seykora JT, Morrisey EE, et al. HDAC1/2 control proliferation and survival in adult epidermis and pre–basal cell carcinoma through p16 and p53. J Invest Dermatol 2022;142:77–87.e10.

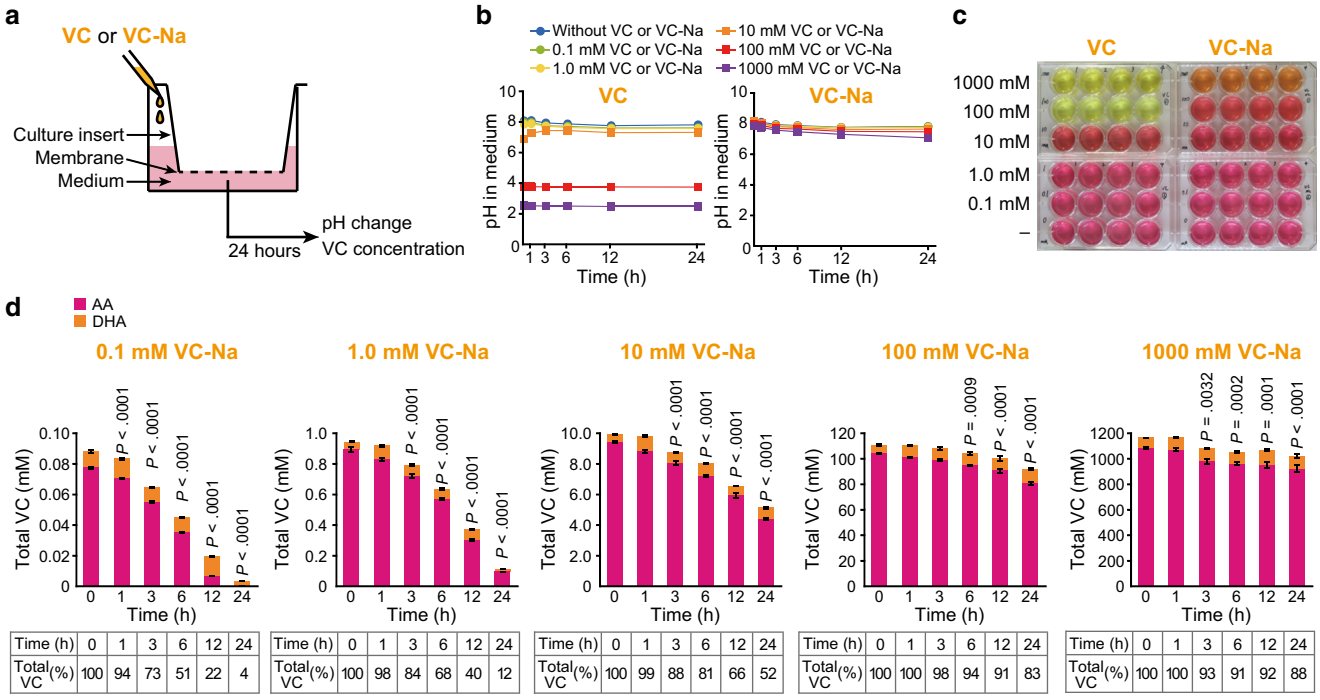

Time (h)	0	1	3	6	12	24
Total VC (%)	100	94	73	51	22	4

Time (h)	0	1	3	6	12	24
Total VC (%)	100	98	84	68	40	12

Time (h)	0	1	3	6	12	24
Total VC (%)	100	99	88	81	66	52

Time (h)	0	1	3	6	12	24
Total VC (%)	100	100	98	94	91	83

Time (h)	0	1	3	6	12	24
Total VC (%)	100	100	93	91	92	88

Supplementary Figure S1. The effect of sodium on pH and the total VC content under experimental conditions. (**a**) Experimental outline for testing the stability of VC or VC sodium salt (denoted as VC-Na) and their ability to change pH in culture medium. The pH was measured at 0, 1, 3, 6, 12, and 24 h, and aliquots of the medium were obtained during the same time periods for measurement of total VC concentrations. (**b**) Changes in the pH of culture medium containing VC or VC-Na (n = 4 per concentration). (**c**) Representative images showing the pH changes in the assay medium using Phenol red as a pH indicator. The image shown is from the 0 h time point, and no apparent changes were observed. (**d**) Total VC concentrations, including AA (red) and DHA (orange) concentrations, in the culture medium (n = 4 per concentration). Statistical analysis of the total VC concentrations was performed. Significance was determined by 1-way ANOVA with the Dunnett posthoc test (for **d**). Source data are provided as a Source Data file. AA, ascorbic acid; DHA, dehydroascorbic acid; h, hour; VC, vitamin C.

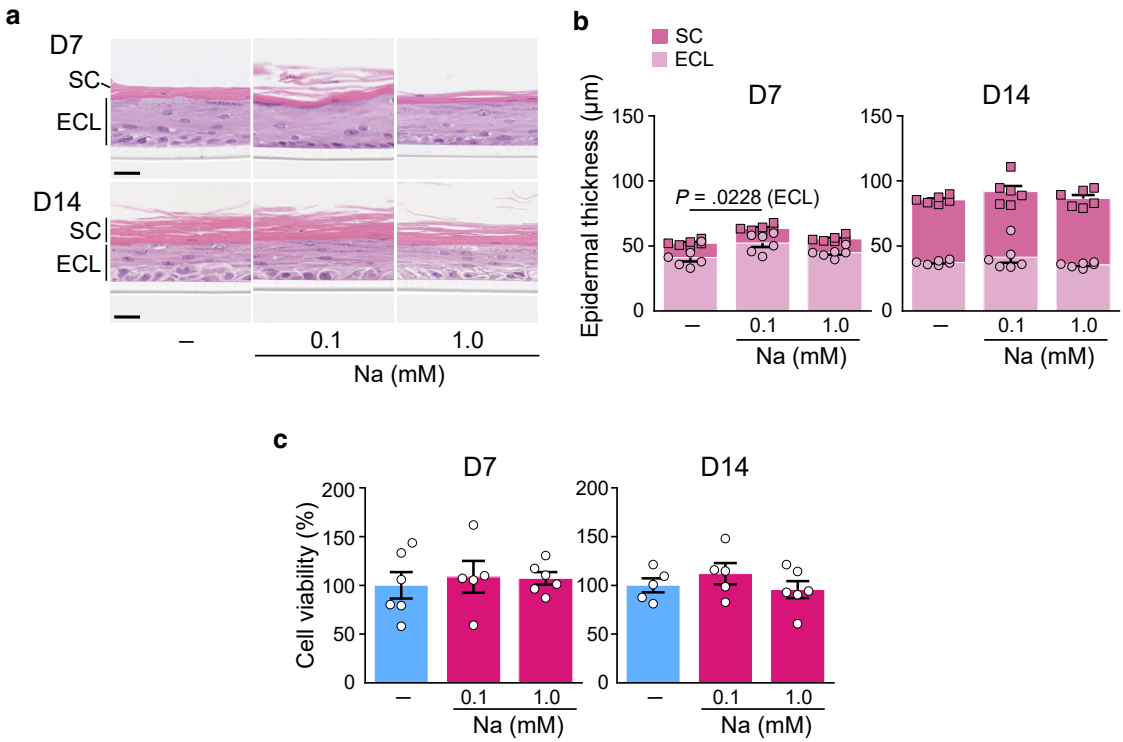

Supplementary Figure S2. The effect of sodium alone on VC-Na–induced phenotypic changes in the human epidermal equivalents. (**a**) Representative H&E images of human epidermal equivalents treated with sodium alone for 7 and 14 days. Bars = 50 μm. (**b**) Quantification of SC (dark pink) and ECL (light pink) thickness in human epidermal equivalents treated with sodium for 7 and 14 days (n = 6). (**c**) There were no significant changes in cell viability of human epidermal equivalents treated with (red) and without (blue) sodium for 7 and 14 days (n = 5–6). Significance was determined by 1-way ANOVA with Tukey's posthoc test (for **b** and **c**). Source data are provided as a Source Data file. ECL, epidermal cell layer; SC, stratum corneum; VC, vitamin C.

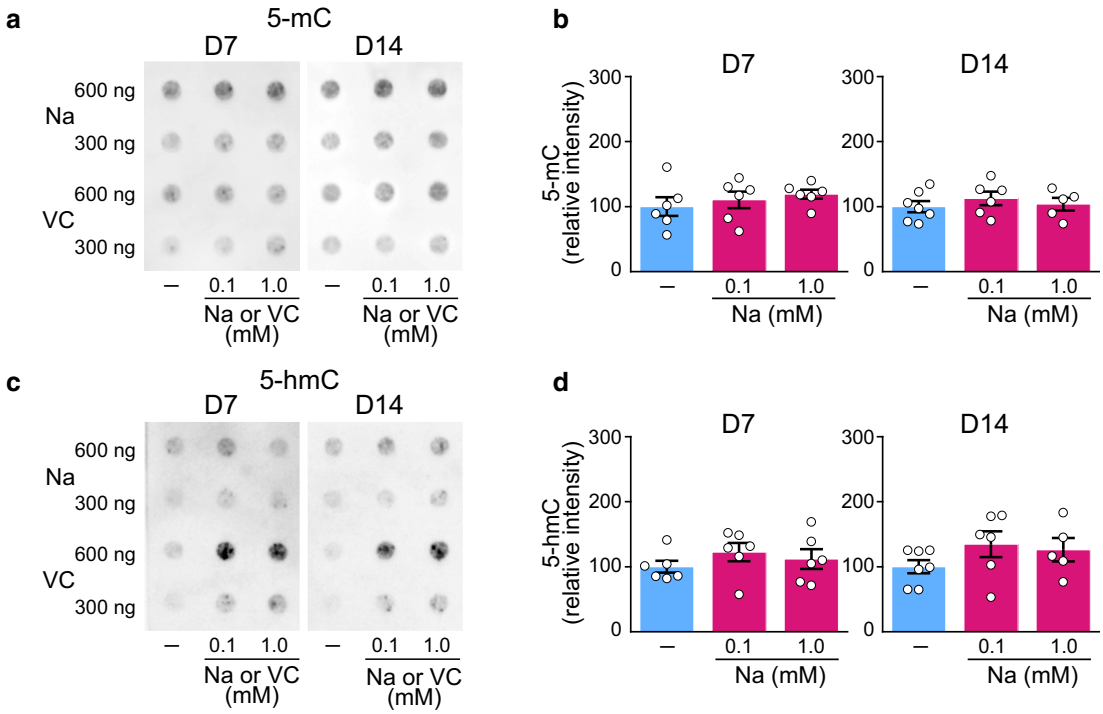

Supplementary Figure S3. The effect of sodium alone on VC-Na–induced DNA methylation changes in the human epidermal equivalents. (**a**) Representative dot blot images showing 5-mC after 7 and 14 days of sodium treatment. (**b**) Semiquantitative analysis of the dot blot assay results for 5-mC. Global 5-mC levels were determined by dot blot analysis of 600 ng of genomic DNA (n = 5–7). (**c**) Representative dot blot images showing 5-hmC after 7 and 14 days of sodium treatment. (**d**) Semiquantitative analysis of the dot blot assay results for 5-hmC. Global 5-hmC levels were determined by dot blot analysis of 600 ng of genomic DNA (n = 5–7). Representative dot blot images showing the effect of VC sodium salt treatment were obtained as a positive control (for **a** and **c**). The red and blue bars in the graphs represent data collected with and without sodium, respectively (for **b** and **d**). Significance was determined by 1-way ANOVA with Tukey's posthoc test (for **b** and **d**). Source data are provided as a Source Data file. 5-hmC, 5-hydroxymethylcytosine; 5-mC, 5-methylcytosine; VC, vitamin C.

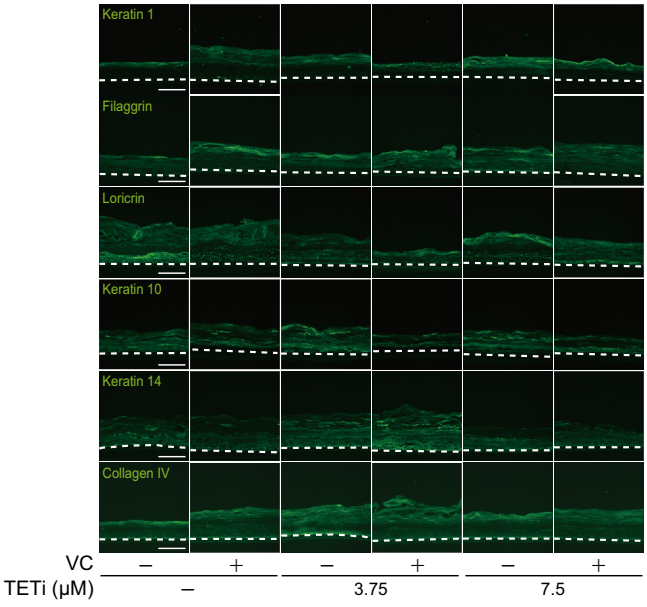

Supplementary Figure S4. Effect of a TET inhibitor on the immunofluorescence staining of differentiation markers. Presented are representative immunofluorescence images showing keratin 1, filaggrin, loricrin, keratin 10, keratin 14, and collagen IV. Bars = 50 μm. The dotted line represents the basement membrane. TET, ten-eleven translocation; VC, vitamin C.

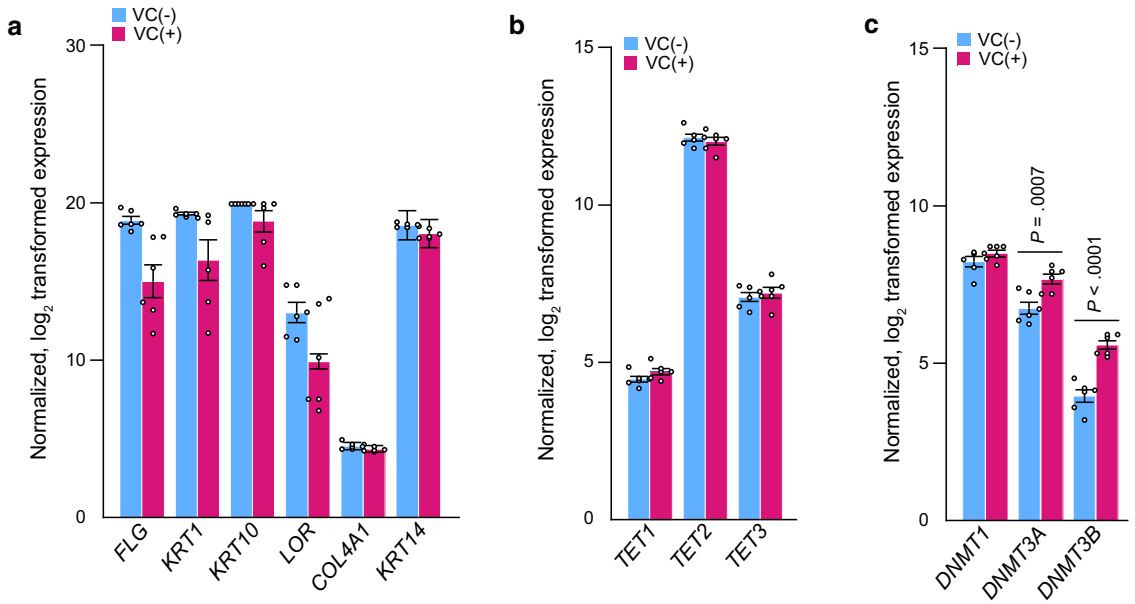

Supplementary Figure S5. Analysis of microarray data from human epidermal equivalents. (**a**) Expression of *FLG, K1, K10, LOR, COL4A1*, and *K14* (n = 6). (**b**) Expression of *TET* genes (n = 6). (**c**) Expression of *DNMT* genes (n = 6). Statistical significance was assessed by the Benjamini–Hochberg method for multiple testing calibrations (for **a**–**c**). Source data are provided as a Source Data file. DNMT, DNA methyltransferase; FLG, filaggrin; K, keratin; LOR, loricrin; TET, ten-eleven translocation; VC, vitamin C.

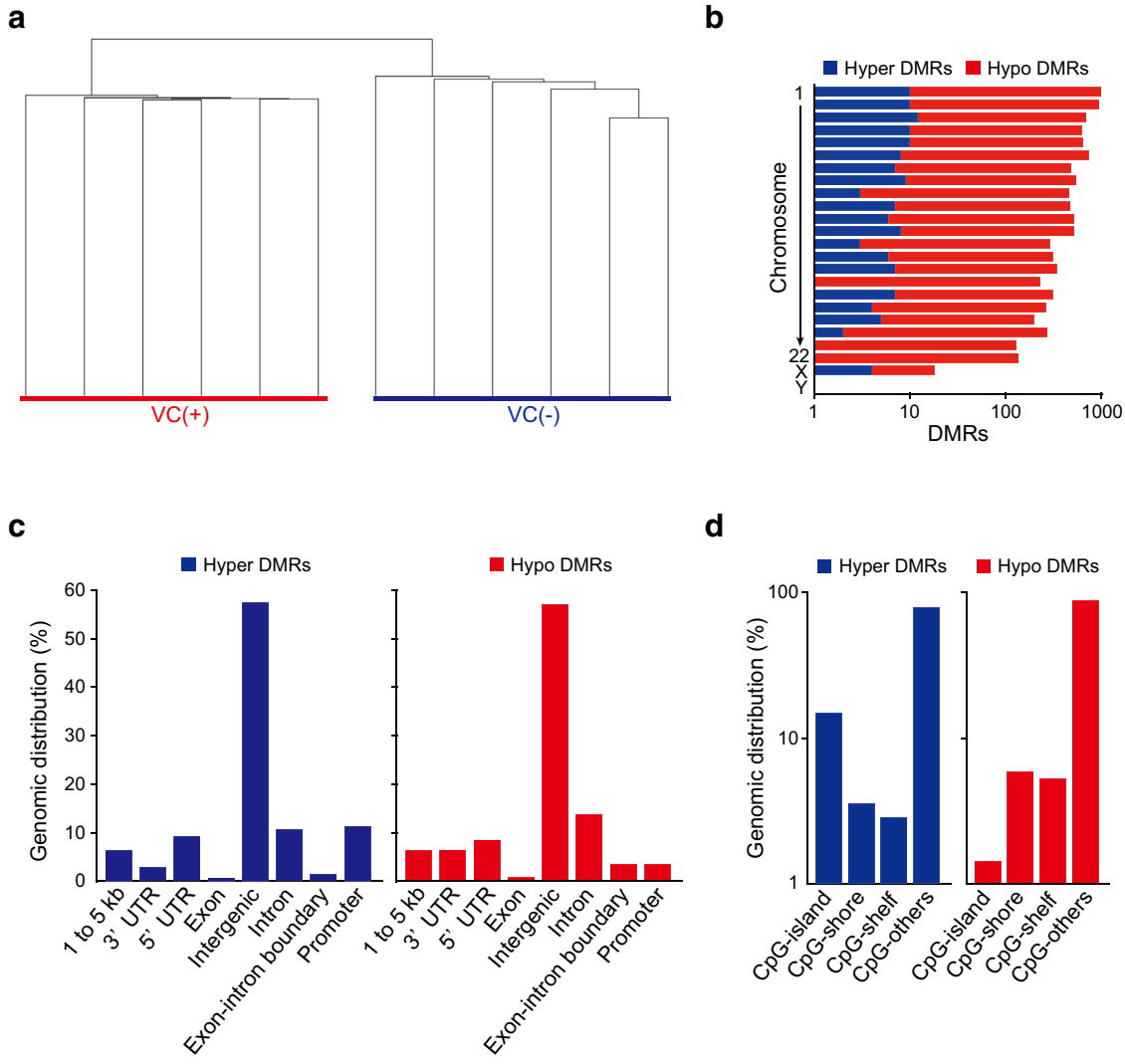

Supplementary Figure S6. Analysis of the DNA methylation profiles of human epidermal equivalents. (**a**) Hierarchical cluster analysis of the methylome profiles of human epidermal equivalents identified significant changes between the VC-treated group and controls (n = 6). (**b**) Distribution of DMRs on chromosomes. (**c**) Genomic distribution of DMRs. (**d**) Distribution of DMRs in CpG context. The longitudinal axis is shown as a log scale (for **b** and **d**). Source data are provided as a Source Data file. DMR, differentially methylated region; UTR, untranslated region; VC, vitamin C.

Supplementary Table S1. Detailed Data for WGBS and Microarray in the 81 Overlapping Genes

Gene Name	Chromosome Number: Start Position–End Position	VC(−)1	VC(−)2	VC(−)3	VC(−)4	VC(−)5	VC(−)6	VC(+)1	VC(+)2	VC(+)3	VC(+)4	VC(+)5	VC(+)6
WGBS													
GSR	chr8:30689001−30690000	0.78	0.94	0.91	1.00	0.91	1.00	0.50	1.00	0.75	0.74	0.53	0.64
LRRFIP1	chr2:237813001−237814000	0.87	0.57	0.58	0.68	0.65	1.00	0.18	0.52	0.40	0.76	0.16	0.52
OR7E14P	chr11:17012001−17013000	0.78	0.74	0.67	0.72	0.67	0.76	0.12	0.45	0.54	0.45	0.39	0.59
ATF7IP2	chr16:10309001−10310000	0.86	0.74	0.76	0.77	0.85	0.93	0.17	0.52	0.43	0.68	0.56	0.56
NTN4	chr12:95654001−95655000	0.35	0.50	0.42	0.57	0.41	0.27	0.14	0.18	0.20	0.07	0.17	0.00
FAP	chr2:162231001−162232000	0.62	0.49	0.45	0.94	0.41	0.34	0.24	0.28	0.23	0.16	0.20	0.24
SVIL	chr10:29780001−29781000	0.52	0.65	0.65	0.90	0.54	0.77	0.42	0.30	0.45	0.41	0.42	0.42
GPCPD1	chr20:5609001−5610000	0.44	0.55	0.50	0.70	0.51	0.62	0.21	0.32	0.37	0.21	0.23	0.34
CEACAM6	chr19:41771001−41772000	0.75	0.66	0.70	0.65	0.72	0.72	0.50	0.42	0.31	0.43	0.44	0.49
GLULP3	hr11:122601001−122602000	0.70	0.57	0.60	0.66	0.61	0.59	0.38	0.40	0.20	0.33	0.40	0.39
GPCPD1	chr20:5608001−5609000	0.64	0.66	0.55	0.59	0.66	0.49	0.37	0.33	0.13	0.15	0.21	0.26
RBM47	chr4:40406001−40407000	0.89	0.78	0.85	0.88	0.84	0.68	0.57	0.42	0.38	0.48	0.39	0.49
EREG	chr4:74364001−74365000	0.66	0.66	0.60	0.62	0.56	0.53	0.37	0.34	0.17	0.34	0.28	0.26
EREG	chr4:74390001−74391000	1.00	0.94	0.93	1.00	0.92	1.00	0.47	0.35	0.51	0.32	0.62	0.68
HNMT	chr2:138023001−138024000	0.53	0.59	0.54	0.51	0.47	0.56	0.23	0.16	0.24	0.04	0.20	0.30
TMPRSS11E	chr4:68456001−68457000	0.95	0.93	0.97	0.93	0.90	0.94	0.71	0.64	0.74	0.54	0.73	0.70
GSAP	chr7:77383001−77384000	0.81	0.75	0.77	0.66	0.69	0.72	0.50	0.39	0.44	0.36	0.42	0.43
NRIP1	chr21:15060001−15061000	0.75	0.75	0.77	0.76	0.74	0.71	0.41	0.18	0.29	0.18	0.19	0.34
OLR1	chr12:10172001−10173000	0.73	0.59	0.65	0.56	0.71	0.59	0.32	0.16	0.22	0.13	0.36	0.37
KYNU	chr2:142875001−142876000	0.68	0.77	0.71	0.71	0.70	0.66	0.46	0.41	0.46	0.30	0.39	0.35
DNMT3B	chr20:32764001−32765000	0.85	0.88	0.84	0.87	0.90	0.89	0.60	0.64	0.63	0.52	0.52	0.59
GPCPD1	chr20:5645001−5646000	0.77	0.80	0.73	0.78	0.77	0.81	0.35	0.31	0.30	0.22	0.23	0.20
BDKRB1	chr14:96257001−96258000	0.63	0.72	0.66	0.83	0.72	0.67	0.43	0.37	0.34	0.21	0.35	0.35
SCARB2	chr4:76177001−76178000	0.63	0.69	0.70	0.64	0.62	0.68	0.43	0.38	0.40	0.34	0.41	0.36
SH3PXD2A-AS1	chr10:103747001−103748000	0.36	0.39	0.39	0.44	0.37	0.43	0.16	0.15	0.12	0.09	0.17	0.12
FAM83A	chr8:12317200−123173000	0.95	0.94	0.94	0.90	0.90	0.88	0.56	0.56	0.54	0.55	0.62	0.60
RAVER2	chr1:64770001−64771000	0.96	0.95	0.89	0.95	0.88	0.87	0.59	0.65	0.67	0.57	0.67	0.65
EMP1	chr12:13209001−13210000	0.50	0.50	0.53	0.49	0.46	0.58	0.07	0.15	0.14	0.02	0.12	0.13
SLC9A8	chr20:49805001−49806000	0.60	0.64	0.65	0.66	0.58	0.62	0.30	0.31	0.31	0.29	0.29	0.33
CYB5R2	chr11:7676001−7677000	0.90	0.93	0.92	0.94	0.93	0.93	0.61	0.67	0.61	0.60	0.62	0.69
TPM1	chr15:63012001−63013000	0.88	0.95	0.93	0.94	0.95	0.95	0.65	0.68	0.65	0.63	0.70	0.68
CEP70	chr3:138558001−138559000	0.93	0.75	0.89	0.91	0.81	0.90	0.60	0.53	0.64	0.58	0.57	0.56
GPR161	chr1:168138001−168139000	0.92	0.82	0.83	0.86	0.78	0.79	0.50	0.48	0.62	0.53	0.53	0.59
GPR161	chr1:168089001−168090000	0.65	0.60	0.50	0.63	0.50	0.47	0.31	0.20	0.35	0.29	0.25	0.20
SH3PXD2A-AS1	chr10:103792001−103793000	0.53	0.48	0.53	0.76	0.51	0.50	0.26	0.25	0.21	0.29	0.28	0.30
RHCG	chr15:89497001−89498000	0.91	0.92	0.84	1.00	0.95	0.86	0.65	0.62	0.63	0.63	0.74	0.63
HDAC1	chr1:32289001−32290000	0.58	0.67	0.75	0.64	0.56	0.71	0.42	0.37	0.34	0.25	0.27	0.39

(*continued*)

Supplementary Table S1. Continued

Gene Name	Chromosome Number: Start Position–End Position	VC(−)1	VC(−)2	VC(−)3	VC(−)4	VC(−)5	VC(−)6	VC(+)1	VC(+)2	VC(+)3	VC(+)4	VC(+)5	VC(+)6
PLEKHA7	chr11:16787001–16788000	0.72	0.71	0.79	0.81	0.71	0.71	0.44	0.47	0.53	0.39	0.40	0.47
PTAFR	chr1:28161001–28162000	0.65	0.78	0.75	0.80	0.65	0.65	0.34	0.12	0.41	0.13	0.19	0.38
POPDC3	chr6:105174001–105175000	0.81	0.80	0.77	0.87	0.78	0.81	0.54	0.59	0.51	0.52	0.47	0.63
SH3PXD2A-AS1	chr10:103782001–103783000	0.79	0.79	0.80	0.86	0.74	0.77	0.59	0.54	0.51	0.50	0.48	0.56
FBXO32	chr8:123526001–123527000	0.84	0.86	0.86	0.91	0.85	0.81	0.59	0.63	0.57	0.47	0.49	0.60
ATP9A	chr20:51636001–51637000	0.84	0.86	0.86	0.85	0.81	0.88	0.52	0.57	0.68	0.53	0.63	0.60
SIDT1	chr3:113537001–113538000	0.87	0.95	0.92	0.93	0.76	0.91	0.46	0.52	0.66	0.44	0.57	0.64
SRD5A3	chr4:55330001–55331000	0.72	0.70	0.72	0.66	0.53	0.66	0.29	0.40	0.39	0.25	0.33	0.35
KATNBL1	chr15:34175001–34176000	0.85	0.90	0.89	0.78	0.79	0.79	0.49	0.52	0.64	0.60	0.45	0.55
LINC01269	chr14:70692001–70693000	0.85	0.82	0.84	0.83	0.68	0.85	0.51	0.45	0.60	0.57	0.39	0.52
MB21D2	chr3:192899001–192900000	0.87	0.85	0.82	0.80	0.75	0.87	0.42	0.52	0.51	0.50	0.35	0.52
BLVRA	chr7:43760001–43761000	0.89	0.90	0.91	0.94	0.99	0.95	0.71	0.68	0.75	0.62	0.56	0.59
KYNU	chr2:142870001–142871000	0.82	0.96	0.95	0.91	0.95	0.93	0.64	0.66	0.64	0.33	0.38	0.35
PALMD	chr1:99682001–99683000	0.84	0.83	0.82	0.94	0.73	0.68	0.61	0.51	0.53	0.35	0.38	0.42
SLC44A3	chr1:94823001–94824000	0.63	0.67	0.62	0.70	0.54	0.53	0.41	0.29	0.42	0.13	0.26	0.29
WNT2B	chr1:112471001–112472000	1.00	0.81	0.86	0.96	0.92	0.92	0.72	0.59	0.76	0.48	0.52	0.55
CAST	chr5:96508001–96509000	0.92	0.94	0.93	0.92	0.93	0.84	0.40	0.51	0.53	0.70	0.71	0.65
TCN1	chr11:59866001–59867000	0.93	0.94	0.94	0.92	0.94	0.88	0.42	0.62	0.66	0.70	0.71	0.71
SOCS2	chr12:93582001–93583000	0.51	0.59	0.56	0.46	0.63	0.55	0.07	0.19	0.15	0.24	0.35	0.28
PAPPA	chr9:116106001–116107000	0.88	0.85	0.82	0.75	0.87	0.80	0.50	0.40	0.63	0.66	0.59	0.57
CAST	chr5:96507001–96508000	0.86	0.87	0.82	0.93	0.81	0.86	0.51	0.38	0.67	0.62	0.78	0.63
CXCL17	chr19:42443001–42444000	0.66	0.61	0.68	0.76	0.61	0.59	0.36	0.30	0.30	0.33	0.42	0.50
EMP1	chr12:13186001–13187000	0.94	0.84	0.95	0.93	0.82	0.91	0.55	0.55	0.49	0.61	0.55	0.73
SVIL	chr10:29730001–29731000	0.80	0.88	0.90	0.93	0.86	0.89	0.54	0.50	0.56	0.65	0.65	0.72
KYNU	chr2:142886001–142887000	0.86	0.85	0.89	0.79	0.93	0.93	0.63	0.45	0.51	0.61	0.55	0.74
CAMK2G	chr10:73872001–73873000	0.52	0.63	0.71	0.59	0.62	0.66	0.35	0.28	0.27	0.40	0.34	0.55
GPCPD1	chr20:5601001–5602000	0.92	1.00	0.94	0.98	0.97	0.93	0.59	0.63	0.71	0.65	0.70	0.69
KATNBL1	chr15:34165001–34166000	0.92	0.87	0.85	0.84	0.84	0.86	0.37	0.41	0.47	0.45	0.39	0.48
RBM47	chr4:40585001–40586000	0.76	0.82	0.85	0.82	0.84	0.77	0.25	0.20	0.37	0.25	0.20	0.31
GPCPD1	chr20:5655001–5656000	0.55	0.52	0.59	0.64	0.64	0.56	0.25	0.28	0.29	0.31	0.30	0.30
TRIOBP	chr22:37782001–37783000	0.53	0.59	0.61	0.59	0.70	0.64	0.07	0.14	0.24	0.24	0.16	0.18
PAPPA	chr9:116142001–116143000	0.31	0.46	0.48	0.43	0.47	0.56	0.10	0.06	0.12	0.10	0.04	0.09
PTAFR	chr1:28169001–28170000	0.75	0.80	0.90	0.85	0.83	0.93	0.47	0.37	0.60	0.51	0.46	0.51
LHFPL2	chr5:78530001–78531000	0.49	0.44	0.53	0.50	0.48	0.45	0.15	0.21	0.21	0.20	0.20	0.34
PALMD	chr1:99627001–99628000	0.78	0.85	0.85	0.83	0.80	0.79	0.49	0.57	0.53	0.51	0.50	0.64
RUNX2	chr6:45682001–45683000	0.76	0.88	0.88	0.88	0.87	0.92	0.44	0.59	0.55	0.51	0.58	0.70

(*continued*)

Supplementary Table S1. Continued

Gene Name	Chromosome Number: Start Position–End Position	VC(−)1	VC(−)2	VC(−)3	VC(−)4	VC(−)5	VC(−)6	VC(+)1	VC(+)2	VC(+)3	VC(+)4	VC(+)5	VC(+)6
NIPAL3	chr1:24393001–24394000	0.60	0.64	0.84	0.93	0.94	0.69	0.55	0.33	0.37	0.40	0.54	0.41
PCSK5	chr9:75925001–75926000	0.69	0.63	0.61	0.69	0.65	0.58	0.51	0.39	0.28	0.59	0.34	0.34
KATNBL1	chr15:34176001–34177000	0.95	0.93	0.95	0.93	0.93	0.94	0.61	0.60	0.58	0.72	0.52	0.63
CSGALNACT1	chr8:19741001–19742000	0.88	0.79	0.83	0.91	0.88	0.79	0.53	0.48	0.55	0.64	0.49	0.56
SRGAP1	chr12:63847001–63848000	0.97	0.97	0.95	0.97	0.98	0.97	0.68	0.65	0.64	0.82	0.65	0.58
EREG	chr4:74370001–74371000	0.86	0.93	0.85	0.90	0.89	0.86	0.34	0.36	0.42	0.56	0.37	0.35
PCSK5	chr9:75915001–75916000	0.82	0.77	0.76	0.86	0.91	0.85	0.54	0.44	0.50	0.45	0.48	0.48
NTN4	chr12:95653001–95654000	0.54	0.54	0.45	0.57	0.59	0.57	0.36	0.30	0.19	0.30	0.23	0.19
GCNT3	chr15:59594001–59595000	0.75	0.74	0.72	0.82	0.87	0.82	0.49	0.51	0.64	0.71	0.48	0.47
TMPRSS11E	chr4:68451001–68452000	1.00	0.57	0.68	0.62	0.63	0.36	0.29	0.21	0.26	0.28	0.28	0.39
GCNT3	chr15:59611001–59612000	0.86	0.42	0.52	0.63	0.48	0.42	0.13	0.41	0.21	0.20	0.30	0.13
GPCPD1	chr20:5582001–5583000	0.94	0.97	0.84	0.88	0.85	0.79	0.54	0.57	0.52	0.44	0.55	0.35
TTC9	chr14:70663001–70664000	0.77	0.79	0.73	0.71	0.77	0.70	0.46	0.48	0.48	0.46	0.43	0.34
LHFPL2	chr5:78769001–78770000	0.86	0.79	0.73	0.72	0.75	0.68	0.46	0.64	0.51	0.53	0.43	0.33
TCN1	chr11:59865001–59866000	0.86	0.95	0.73	0.76	1.00	0.48	0.53	0.55	0.43	0.39	0.29	0.44
APOL4	chr22:36201001–36202000	0.52	0.60	0.75	0.63	0.38	0.39	0.12	0.41	0.28	0.28	0.32	0.48
MB21D2	chr3:192862001–192863000	0.63	0.66	0.60	0.63	0.52	0.52	0.22	0.33	0.33	0.30	0.38	0.38
PAPPA	chr9:116104001–116105000	0.83	0.81	0.72	0.88	0.38	0.64	0.08	0.26	0.28	0.34	0.30	0.25
LY6D	chr8:142785001–142786000	0.51	0.68	0.54	0.53	0.39	0.35	0.20	0.20	0.29	0.31	0.21	0.35
PALMD	chr1:99662001–99663000	0.52	0.48	0.61	0.50	0.39	0.54	0.21	0.27	0.13	0.15	0.32	0.43
FBXO32	chr8:123530001–123531000	0.69	0.81	0.82	0.69	0.79	0.81	0.17	0.63	0.26	0.44	0.64	0.58
RASSF6	chr4:73611001–73612000	0.20	0.61	0.41	0.34	0.28	0.38	0.00	0.11	0.00	0.08	0.00	0.07
GSR	chr8:30717001–30718000	0.81	0.83	0.84	0.76	0.73	0.77	0.31	0.52	0.15	0.45	0.53	0.34
PAPPA	chr9:116190001–116191000	0.76	0.78	0.73	0.88	0.78	0.83	0.46	0.56	0.39	0.57	0.51	0.47
ITGB8	chr7:20410001–20411000	0.63	0.68	0.68	0.66	0.70	0.73	0.33	0.36	0.24	0.44	0.35	0.40
CYP1B1	chr2:38092001–38093000	0.70	0.69	0.69	0.63	0.66	0.82	0.29	0.39	0.29	0.50	0.38	0.33
ZBTB38	chr3:141332001–141333000	0.75	0.78	0.78	0.72	0.72	0.79	0.34	0.46	0.35	0.56	0.37	0.34
LINC01269	chr14:70698001–70699000	0.83	0.83	0.84	0.79	0.79	0.91	0.45	0.72	0.53	0.53	0.55	0.54
CAMK2G	chr10:73881001–73882000	0.91	0.98	0.89	0.85	0.81	0.95	0.41	0.69	0.85	0.46	0.53	0.52
TMPRSS11B	chr4:68244001–68245000	0.63	0.76	0.77	0.68	0.81	0.74	0.44	0.55	0.48	0.36	0.52	0.47
DHRS3	chr1:12602001–12603000	0.95	0.92	0.93	0.90	0.91	0.90	0.54	0.77	0.73	0.43	0.72	0.66
PAPPA	chr9:116087001–116088000	0.49	0.56	0.45	0.32	0.40	0.31	0.09	0.12	0.11	0.06	0.08	0.13
MECOM	chr3:169186001–169187000	0.79	0.83	0.59	0.53	0.70	0.62	0.22	0.29	0.51	0.30	0.32	0.55
OR8R1P	chr11:73249001–73250000	0.81	0.80	0.71	0.79	0.83	0.63	0.41	0.52	0.51	0.46	0.44	0.66
MYLK	chr3:123616001–123617000	0.95	0.77	0.80	0.91	0.79	0.69	0.41	0.50	0.44	0.46	0.49	0.57
NRIP1	chr21:15061001–15062000	0.92	0.86	0.86	0.73	0.69	0.87	0.63	0.42	0.73	0.35	0.59	0.61
ANKRD29	chr18:23651001–23652000	0.69	0.68	0.68	0.59	0.56	0.77	0.39	0.04	0.42	0.24	0.30	0.43
ERV3-1	chr7:64990001–64991000	0.97	0.82	0.82	0.71	0.69	0.91	0.48	0.43	0.65	0.38	0.42	0.60

(*continued*)

Supplementary Table S1. Continued

Gene Name	Chromosome Number: Start Position–End Position	VC(−)1	VC(−)2	VC(−)3	VC(−)4	VC(−)5	VC(−)6	VC(+)1	VC(+)2	VC(+)3	VC(+)4	VC(+)5	VC(+)6
SH3PXD2A-AS1	chr10:103777001−103778000	0.53	0.49	0.48	0.37	0.35	0.55	0.29	0.20	0.23	0.16	0.18	0.26
GSR	chr8:30722001−30723000	0.61	0.47	0.34	0.41	0.46	0.51	0.17	0.18	0.21	0.07	0.20	0.19
TCN1	chr11:59857001−59858000	0.56	0.61	0.54	0.44	0.51	0.67	0.30	0.33	0.32	0.20	0.29	0.29
SH3PXD2A-AS1	chr10:103761001−103762000	0.78	0.77	0.72	0.54	0.49	0.80	0.45	0.45	0.22	0.21	0.33	0.36
C15orf48	chr15:45450001−45451000	0.82	0.87	0.79	0.75	0.65	0.88	0.39	0.46	0.24	0.17	0.57	0.41
CLMP	chr11:123197001−123198000	0.58	0.41	0.44	0.48	0.32	0.81	0.13	0.31	0.23	0.12	0.00	0.45
PTAFR	chr1:28151001−28152000	0.90	0.89	0.88	0.98	0.93	0.97	0.60	0.74	0.71	0.50	0.56	1.00
SOX9	chr17:72126001−72127000	0.44	0.79	0.75	0.56	0.75	0.66	0.82	0.37	0.38	0.42	0.31	0.30
EREG	chr4:74368001−74369000	0.46	0.65	0.63	0.79	0.55	0.71	0.63	0.00	0.31	0.20	0.19	0.13
DNMT3B	chr20:32765001−32766000	0.59	0.83	0.79	0.32	0.61	0.64	0.44	0.32	0.57	0.25	0.16	0.10
ROS1	chr6:117389001−117390000	0.49	0.69	0.55	0.44	0.63	0.58	0.24	0.20	0.22	0.26	0.30	0.23
GPCPD1	chr20:5647001−5648000	0.59	0.67	0.70	0.41	0.75	0.66	0.35	0.42	0.25	0.32	0.31	0.38
TRIOBP	chr22:37698001−37699000	0.48	0.66	0.67	0.53	0.78	0.75	0.49	0.31	0.25	0.35	0.28	0.33
OLR1	chr12:10178001−10179000	1.00	0.92	0.86	0.90	0.97	0.96	0.68	0.54	0.88	0.56	0.90	0.48
GALNT3	chr2:165775001−165776000	0.17	0.67	0.58	1.00	0.74	0.63	0.04	0.15	0.55	0.09	0.61	0.33
RBM47	chr4:40653001−40654000	0.62	0.62	0.58	0.08	0.56	0.58	0.20	0.28	0.27	0.47	0.37	0.52
MTND5P15	chr3:176950001−176951000	0.67	0.59	0.67	0.00	0.29	0.72	0.03	0.00	0.41	0.07	0.12	0.85
CXCL8	chr4:73753001−73754000	1.00	0.43	0.25	0.00	0.90	0.00	0.00	0.00	0.00	1.00	0.00	0.06
ATF7IP2	chr16:10278001−10279000	0.80	0.79	0.69	0.74	0.60	0.11	0.20	0.34	0.66	0.60	0.34	0.58
Microarray													
MYLK	—	5.30	5.51	5.33	5.60	5.40	5.90	6.54	5.87	6.54	6.11	6.50	5.91
NIPAL3	—	6.60	6.48	6.37	6.57	6.63	6.80	7.54	7.40	6.79	7.20	7.50	7.17
NTN4	—	7.13	6.70	6.57	6.98	7.19	7.35	9.48	8.96	8.15	8.87	9.16	8.12
TMPRSS11B	—	3.97	4.99	3.56	3.91	5.77	5.45	8.48	7.22	6.16	7.68	8.80	6.52
FBXO32	—	6.81	6.85	6.17	6.61	7.06	6.82	8.12	7.60	7.16	7.87	8.08	7.26
OR7E14P	—	4.85	4.72	4.96	4.76	4.64	4.98	7.13	5.98	5.63	6.16	6.45	5.79
DHRS3	—	7.98	8.14	7.93	7.82	8.06	8.02	9.90	8.79	8.57	9.61	9.56	8.71
CXCL17	—	6.81	6.92	6.44	6.19	6.37	6.53	9.23	7.81	7.49	7.72	9.04	7.63
EMP1	—	8.13	7.79	7.74	8.18	8.03	8.78	10.36	9.17	8.49	10.09	9.90	8.99
TTC9	—	7.13	6.76	6.28	6.56	7.30	7.22	9.04	7.85	7.67	8.90	8.60	7.95
TPM1	—	7.11	6.42	6.51	6.80	7.12	7.07	8.67	7.64	7.49	8.58	8.57	7.34
MECOM	—	4.93	4.09	4.14	4.56	4.56	4.88	5.73	5.32	5.15	5.62	6.26	5.47
PTAFR	—	5.66	5.32	5.41	5.39	5.53	5.76	6.43	6.00	5.74	6.08	6.50	6.18
GLULP3	—	9.03	8.87	8.81	8.90	8.91	9.05	9.88	9.50	9.15	9.72	9.96	9.52
RHCG	—	9.20	9.57	9.35	9.24	9.72	9.40	10.93	10.75	10.46	11.03	11.07	10.74
PALMD	—	7.92	7.74	7.43	7.65	7.93	7.74	8.74	8.58	8.60	8.74	8.92	8.68
CAST	—	9.65	9.42	9.42	9.54	9.73	9.56	10.23	10.16	10.13	10.27	10.23	10.20
GCNT3	—	5.79	6.11	5.39	6.04	6.45	6.10	7.91	8.26	8.06	8.20	8.29	7.87

(*continued*)

Supplementary Table S1. Continued

Gene Name	Chromosome Number: Start Position–End Position	VC(−)1	VC(−)2	VC(−)3	VC(−)4	VC(−)5	VC(−)6	VC(+)1	VC(+)2	VC(+)3	VC(+)4	VC(+)5	VC(+)6
PLEKHA7	—	6.03	6.08	5.95	6.05	6.35	6.20	6.84	6.80	6.48	6.62	6.77	6.47
FAM83A	—	8.38	8.44	8.23	8.39	8.92	8.81	9.68	9.52	9.13	9.30	9.48	9.52
CEACAM6	—	8.34	9.33	8.42	9.47	9.96	9.77	11.25	10.94	10.75	11.09	11.39	10.75
RUNX2	—	6.52	6.00	6.12	6.28	6.62	6.33	7.30	6.86	6.88	7.12	7.29	6.74
ITGB8	—	7.29	6.66	6.56	7.51	7.64	7.33	9.29	8.55	8.56	9.14	9.01	7.85
C15orf48	—	7.25	6.92	7.09	7.41	7.89	7.61	9.24	8.11	8.13	8.80	8.69	8.19
SOX9	—	7.11	7.07	6.91	7.27	7.42	7.20	8.32	7.82	7.73	8.13	8.07	7.74
PAPPA	—	5.31	4.92	4.90	5.69	5.49	5.65	6.29	6.39	6.26	6.43	6.34	6.01
GSR	—	7.40	6.66	7.08	7.31	7.30	7.45	8.02	7.99	7.89	8.45	8.19	7.40
SCARB2	—	7.40	6.91	6.90	6.95	7.36	6.94	7.83	7.64	7.52	7.71	7.68	7.65
PCSK5	—	6.06	5.50	5.16	5.51	6.09	5.93	6.92	6.97	6.83	7.22	6.96	6.30
MTND5P15	—	4.14	3.70	3.56	3.52	4.18	3.97	4.63	4.97	4.67	4.81	4.98	4.45
RBM47	—	7.79	7.71	7.55	7.43	7.93	7.85	8.60	8.47	8.20	8.25	8.50	8.25
TMPRSS11E	—	8.86	9.01	8.71	8.53	9.22	9.17	10.63	10.08	9.78	10.18	10.55	10.03
SRGAP1	—	6.12	5.93	5.59	5.67	6.26	6.38	7.17	6.67	6.60	6.87	6.90	6.69
HDAC1	—	8.44	8.12	8.24	8.20	8.49	8.59	9.07	8.93	8.76	8.96	9.08	9.00
ANKRD29	—	6.74	6.28	6.45	6.50	6.86	6.92	7.72	7.49	7.21	7.60	7.75	7.30
GPCPD1	—	5.46	4.62	4.49	4.51	5.44	5.45	7.29	6.72	6.36	7.08	6.92	6.60
DNMT3B	—	5.06	4.47	4.86	4.36	5.07	5.44	6.31	6.12	5.84	5.80	6.19	5.70
ZBTB38	—	8.53	7.96	8.29	8.00	8.38	8.60	9.47	9.07	8.97	9.09	9.19	8.84
LHFPL2	—	6.88	6.52	6.61	6.44	6.94	6.78	7.68	7.28	7.26	7.30	7.49	7.13
RAVER2	—	6.18	5.67	5.93	5.84	6.20	6.03	7.19	6.59	6.42	6.76	6.86	6.39
FAP	—	6.03	4.90	5.91	5.16	6.26	6.22	8.07	6.96	6.79	7.09	7.19	6.76
SVIL	—	6.54	6.47	6.41	6.61	6.98	6.71	7.54	7.67	7.40	7.12	7.61	7.35
MB21D2	—	6.26	5.90	5.82	5.93	6.53	6.46	7.05	7.06	6.82	6.65	7.05	6.91
POPDC3	—	5.78	5.43	5.44	5.37	6.38	6.26	7.23	6.95	7.08	6.71	6.86	6.41
SLC44A3	—	5.94	5.45	5.67	5.86	6.29	5.96	6.72	6.55	6.57	6.18	6.65	6.39
GALNT3	—	8.59	8.02	8.48	8.38	8.86	8.77	9.44	9.25	9.19	9.05	9.17	9.02
RASSF6	—	4.78	3.94	4.40	4.46	5.31	4.64	5.98	5.46	5.50	5.51	5.82	5.68
HNMT	—	5.43	4.48	5.00	5.40	5.85	5.48	6.73	6.02	6.43	6.10	6.61	6.36
CAMK2G	—	7.15	6.49	6.74	6.95	7.33	7.08	8.05	7.45	7.47	7.58	7.82	7.55
SLC9A8	—	6.14	6.17	6.02	5.87	6.08	6.29	6.74	6.62	6.44	6.51	6.58	6.78
CYB5R2	—	9.71	9.79	9.61	9.42	9.66	9.61	10.47	10.19	10.00	10.12	10.36	10.37
LINC01269	—	5.85	5.77	5.60	5.64	6.10	6.17	7.04	6.81	6.13	6.33	6.97	6.74
ATP9A	—	7.07	6.17	6.51	6.12	7.01	6.86	7.77	7.66	7.26	7.15	7.43	7.71
KATNBL1	—	7.38	6.39	6.68	6.42	7.15	7.16	8.02	8.01	7.69	7.23	7.95	7.80
EREG	—	8.01	7.61	7.51	7.18	7.94	7.67	8.66	8.74	8.53	8.04	8.59	8.42
WNT2B	—	4.72	4.07	4.33	4.28	4.22	4.84	5.55	4.82	5.21	5.35	5.39	5.37

(*continued*)

Supplementary Table S1. Continued

Gene Name	Chromosome Number: Start Position–End Position	VC(−)1	VC(−)2	VC(−)3	VC(−)4	VC(−)5	VC(−)6	VC(+)1	VC(+)2	VC(+)3	VC(+)4	VC(+)5	VC(+)6
CEP70	—	5.99	5.07	5.09	5.18	5.76	5.81	7.10	6.48	6.68	6.30	6.61	6.50
CLMP	—	7.10	6.50	6.46	6.62	7.07	7.03	8.35	7.73	7.98	7.62	8.03	7.91
LRRFIP1	—	7.64	7.25	7.32	7.17	7.48	7.52	8.26	7.94	7.87	7.81	7.93	8.21
BLVRA	—	7.37	6.91	6.97	6.71	7.06	7.27	8.48	7.90	7.78	7.88	8.18	8.04
SRD5A3	—	8.67	8.15	7.96	8.00	8.70	8.43	9.81	9.41	9.14	9.20	9.94	9.54
TRIOBP	—	8.27	7.68	7.63	7.57	7.99	8.00	8.89	8.64	8.48	8.26	8.83	8.74
KYNU	—	6.66	5.67	5.80	6.20	6.33	6.06	8.20	7.19	7.08	6.90	7.85	7.50
BDKRB1	—	7.45	7.27	7.09	7.24	7.35	7.27	7.97	7.67	7.63	7.63	7.77	7.77
GSAP	—	5.91	5.58	5.68	5.56	5.57	5.60	6.82	6.10	5.95	6.32	6.11	6.56
SOCS2	—	5.90	5.49	5.49	5.75	6.10	5.83	7.59	6.56	6.14	6.76	6.56	6.91
CSGALNACT1	—	4.75	4.85	4.48	4.94	5.97	5.65	6.22	7.02	7.31	6.64	6.91	7.02
ERV3−1	—	7.74	7.13	7.24	7.33	8.05	7.67	7.98	8.57	8.71	8.11	8.61	8.59
ROS1	—	3.37	3.56	3.52	3.26	4.02	3.95	4.65	4.79	5.26	4.02	4.77	4.31
APOL4	—	6.17	6.25	6.03	5.87	6.08	5.99	6.63	7.28	6.88	6.37	6.63	6.99
CXCL8	—	6.77	6.59	6.66	6.58	6.87	6.67	7.54	7.71	7.50	7.34	7.66	7.97
NRIP1	—	8.63	8.76	8.64	8.66	8.89	8.89	9.49	9.49	9.38	9.25	9.50	9.74
TCN1	—	9.26	9.09	8.96	8.82	9.56	9.21	9.71	9.83	9.92	9.62	9.83	9.97
SH3PXD2A−AS1	—	7.74	7.60	7.22	7.24	7.71	7.83	8.34	8.62	8.58	8.03	8.58	8.83
LY6D	—	7.67	7.59	7.30	7.42	8.01	7.96	8.11	8.75	8.68	8.87	9.15	8.55
OR8R1P	—	3.10	3.09	2.98	3.14	3.22	3.03	3.37	3.92	3.94	3.92	4.32	3.46
ATF7IP2	—	4.27	3.45	4.55	3.90	4.24	4.32	4.89	5.03	4.86	4.84	5.47	4.84
GPR161	—	4.87	4.51	4.67	4.55	4.37	4.71	5.38	5.44	5.03	5.10	5.24	4.95
OLR1	—	6.39	6.43	6.46	5.78	6.07	5.57	8.40	7.66	7.99	7.64	8.36	8.47
CYP1B1	—	4.33	4.16	4.73	4.17	4.11	4.53	6.02	5.73	5.89	5.16	6.11	5.71
SIDT1	—	5.40	5.51	5.40	5.43	5.27	5.28	5.91	6.10	6.13	5.93	6.22	5.93

Abbreviation: WGBS, whole-genome bisulfite sequencing.

Supplementary Table S2. Functions for the 12 Cell Proliferation–Related Genes Identified in Microarray and WGBS

Symbol	Gene Name	Gene ID	TET-Related References	Epidermal-Related References	Proliferation-Related Reference	Reference
CAST	calpastatin	ENSG00000153113		○	○	Lin et al, 2015; Nian and Ma, 2021
CYP1B1	cytochrome P450, family 1, subfamily B, polypeptide 1	ENSG00000138061		○	○	Kwon et al, 2016; Reiners et al, 1998
EMP1	epithelial membrane protein 1	ENSG00000134531	○	○	○	Ichiyama et al, 2015; Li et al, 2015
EREG	epiregulin	ENSG00000124882		○	○	Iwata et al, 2021
FAM83A	family with sequence similarity 83, member A	ENSG00000147689		○	○	Ji et al, 2021; Uchiyama et al, 2019
FBXO32	F-box protein 32	ENSG00000156804	○	○	○	Cai et al, 2020; Habel et al, 2021; Sun et al, 2018
HDAC1	histone deacetylase 1	ENSG00000116478	○	○	○	Zheng et al, 2016; Zhu et al, 2022
NTN4	netrin 4	ENSG00000074527		○	○	Lv et al, 2015; Schneiders et al, 2007
RHCG	Rh family, C glycoprotein	ENSG00000140519		○	○	Chen et al, 2020; Zhang et al, 2021
ROS1	ROS proto-oncogene 1, receptor tyrosine kinase	ENSG00000047936		○	○	Kumar et al, 2018; Lichtenberger et al, 2013
RUNX2	runt-related transcription factor 2	ENSG00000124813	○	○	○	Glotzer et al, 2008; Kawane et al, 2018; Yang et al, 2018
SOX9	SRY box 9	ENSG00000125398		○	○	Shi et al, 2013

Abbreviations: ID, identification; WGBS, whole-genome bisulfite sequencing.

Supplementary Table S3. Primer Sets Used for qPCR Analysis

Gene	Forward Primer Sequence (5′−3′)	Reverse Primer Sequence (5′−3′)
CAST	AATCGCCTTCCAAACCAGGA	AGAGGAAGCTGACACCTTGG
CYP1B1	TCCTCCTCTTCACCAGGTATCC	CTCTGCTGGTCAGGTCCTTG
EMP1	CCCTCCTGGTCTTCGTGT	GGAATAGCCGTGGTGATA
EREG	ATGGCTATTGTTTGCATGGAC	CTCTGGATCCCCTGAGGTAAC
FAM83A	CTCGGACTGGAGATTTGTCC	GGAACTCCTCGTCAAACAGC
FBXO32	GTGAGCGACCTCAGCAGTTA	AGGCAGGCCGGACCA
HDAC1	GACCGACTGACGGTAGGGA	TGGCTTTGTGAGGGCGATAG
NTN4	ATGCTTGCAAACCGTGTTCC	GTCGACAGCCATAGTCTCCG
RHCG	GGTCTACTGGGAGATGCCTG	CCTGCCCTGGGAGCCTA
ROS1	GCCAGCTAGTGAACCACCAT	ATCCCCAGTGCTGCTCTGTC
RUNX2	GCCTTCAAGGTGGTAGCCC	AAGGTGAAACTCTTGCCTCGTC
SOX9	GCAAGCTCTGGAGACTTCTG	CGCCTTGAAGATGGCGTTG
18S rRNA	GGACATCTAAGGGCATCACAG	GAGACTCTGGCATGCTAACTAG

Abbreviation: ribosomal RNA.